Earth-Science Reviews 210 (2020) 103332

Contents lists available at ScienceDirect

Earth-Science Reviews

journal homepage: www.elsevier.com/locate/earscirev

Review Article

Catastrophic soil loss associated with end-Triassic deforestation

B. van de Schootbrugge[a,*], C.M.H. van der Weijst[a], T.P. Hollaar[a,1], M. Vecoli[b], P.K. Strother[c], N. Kuhlmann[d], J. Thein[d], H. Visscher[a], H. van Konijnenburg-van Cittert[a], M.A.N. Schobben[a], A. Sluijs[a], S. Lindström[e]

[a] Department of Earth Sciences, Utrecht University, Marine Palynology & Paleoceanography, Princetonlaan 8a, 3584, CB, Utrecht, the Netherlands
[b] Exploration Technical Services Department, Saudi Aramco, Dhahran, Saudi Arabia
[c] Weston Observatory, Boston College, United States
[d] Institute for Geology, University of Bonn, Nussallee 8, 53115 Bonn, Germany
[e] GEUS–Geological Survey of Denmark and Greenland, Øster Voldgade 10, DK-1350 Copenhagen, Denmark

ABSTRACT

Soils are a crucial link between the atmosphere, biosphere, and geosphere. Any disturbance to the health of soils will severely impact plants as well as a multitude of organisms living in or on soils, such as fungi, bacteria, and insects. Catastrophic soil loss is thought to have played a pivotal role during mass-extinction events as a result of major deforestation, but the exact feedbacks remain elusive. Here, we assess the role of soil loss during the end-Triassic mass-extinction event based on proxy data obtained from four sediment sections recovered from France, Germany, and Denmark. Clay mineral and palynological data indicate a strong increase in erosion during the latest Rhaetian with the influx of kaolinite and abundantly reworked Palaeozoic and Neoproterozoic organic matter. Based on a new timeline, these changes were coeval with intense volcanic activity in the Central Atlantic Magmatic Province (CAMP). In addition to vegetation dieback, repeated forest fires, as well as widespread seismic activity related to CAMP emplacement led to landscape destruction triggering removal of soils. The biological degradation of fern spore walls by fungi and bacteria, a process coupled to organic matter decay in soils, strongly decreased across the T/J boundary. We interpret this counter-intuitive result as evidence for rapid and widespread removal of soils. Taken together, CAMP induced environmental changes led to profound changes in erosion and removal of soils, while soil resilience during the Hettangian appears to have proceeded hand in hand with recovery in Jurassic seas.

1. Introduction

Soils are a key factor in the health of global ecosystems. Acting as an interface between the atmosphere, geosphere, and biosphere, soil biodiversity is likely higher than diversity in above-ground ecosystems (Freckman et al., 1997; Orgiazzi et al., 2016). Not only do soils play a vital role in influencing plant diversity, but healthy soils are also characterized by diverse communities of among others fungi, bacteria, arthropods, and nematodes that together control nutrient fluxes in and out of soils. Many of these interactions reinforce each other with plants actively shaping soil formation, chemistry, and retention of nutrients (Drever, 1994; Van Nuland et al., 2016). In addition, soils store very large quantities of carbon that upon loss can be released to the atmosphere and oceans (Scharlemann et al., 2014).

Soil formation is not only a biological process, but it is closely tied to the chemical weathering of crystalline rock at the Earth's surface, which drives large-scale patterns in mineralogy of clay particle assemblages (Nesbitt and Young, 1984). Chemical weathering depends on bedrock mineralogy, texture, permeability, and the age of the substrate, as well as prevailing climatic conditions, mainly temperature and runoff, and the type of vegetation cover (Nesbitt and Young, 1984; Drever, 1994). Weathering of continental landmasses is thus a prerequisite to form soils in the first place and should be clearly distinguished from erosion, which is the physical removal and transport of regolith and soil by gravity, wind, water or ice.

Soil loss via erosion is the most extreme form of soil disturbance, which can trigger profound changes in ecosystems. Catastrophic soil loss can be due to several mechanisms, including earthquakes and forest fires, but the foremost disturbance is deforestation. Loss of vegetation cover leads to rapid removal of topsoils during rainfall. Today, elevated rates of erosion are, for example, particularly evident on Madagascar where anthropogenic destruction of tropical rainforests leads to extreme soil loss (Cox et al., 2010). Extensive sediment plumes can be seen entering the Indian Ocean using satellite imagery; the landscape of Madagascar proverbally “bleeds to death” as astronauts on the ISS remarked in 2004 while observing the Betsiboka estuary (see also https://earthobservatory.nasa.gov/images/4388/betsiboka-estuary-madagascar).

* Corresponding author.
E-mail address: b.vanderschootbrugge@uu.nl (B. van de Schootbrugge).
[1] Now at the University of Exeter, Exeter, United Kingdom.

https://doi.org/10.1016/j.earscirev.2020.103332
Received 9 December 2019; Received in revised form 25 August 2020; Accepted 26 August 2020
Available online 01 September 2020

In currently accepted scenarios for the end-Permian and end-Triassic extinctions, deforestation and soil loss are key triggers driving the extinction of species on land and likely played a role in the eutrophication and spread of shallow marine anoxia (Visscher et al., 1996; Looy et al., 2001; Algeo and Twitchett, 2010; Algeo et al., 2011a). Hence, soil loss is regarded as a crucial link between ecosystem disturbance on land and in the oceans. Elevated erosion rates associated with the end-Permian extinction have been inferred from a wealth of information on changes in river morphology (Smith, 1995; Retallack et al., 2006; Newell et al., 2010; Zhu et al., 2019), as well as strong increases in sediment fluxes (Algeo and Twitchett, 2010; Algeo et al., 2011b). Influx of soil-derived organic debris and organic biomarkers has been attributed to increased soil erosion (Sephton et al., 2005a, 2005b; Wang and Visscher, 2007; French et al., 2012; Sawada et al., 2012; Kaiho et al., 2016). Eutrophication and widespread anoxia, including photic zone euxinia, were likely important proximate kill mechanisms that contributed to the extinction of Permian marine invertebrates (Isozaki, 1997; Grice et al., 2005; Isozaki et al., 2007; Shen et al., 2007; Wignall et al., 2010; Kaiho and Koga, 2013).

For the end-Triassic extinction, many of the general triggers and feedback mechanisms that contributed to extinction (van de Schootbrugge and Wignall, 2016) have been implicated in recently published detailed studies, including work on country-rock basalt interactions in the CAMP province (Heimdal et al., 2018), carbon cycle perturbations (Bacon et al., 2011; Ruhl et al., 2011; Ruhl and Kürschner, 2011), terrestrial devastation (Lindström et al., 2012; 2016), possible effects of sulfuric acid on leaf roundness and plant cuticles (Bacon et al., 2011; Steinthorsdottir et al., 2017), increases in pCO_2 (Steinthorsdottir et al., 2011), and photic zone euxinia (Richoz et al., 2012; Jaraula et al., 2013; Kasprak et al., 2015) as well as widespread anoxia (Jost et al., 2017; Luo et al., 2018). Based on a marked change in fluvial style in East Greenland, Steinthorsdottir et al. (2012) argued for an increase in run-off, which was perhaps driven by a global decrease in evapotranspiration and an associated increase in humidity, as indicated by lower stomatal densities on plant leaves. A dominance of C_{29} steranes in sedimentary organic matter from the marine Kennecott Point section on the Haida Gwaii Islands, Canada, suggests that the main carbon source was from land (Jiao et al., 2008). Deforestation is also implicated in the end-Triassic mass-extinction event (van de Schootbrugge et al., 2009; van de Schootbrugge and Wignall, 2016), however its effect on soil erosion remains largely unaddressed and difficult to quantify.

Analyses of micro- and macrofloral abundance and diversity indicate severe changes in land plant cover during the latest Rhaetian in NW Europe (van de Schootbrugge et al., 2009; van de Schootbrugge and Wignall, 2016), Greenland (McElwain et al., 1999), and North America (Cirilli et al., 2009; Fowell et al., 1994). Detailed palynological studies of cores and outcrops in Denmark (Lindström et al., 2012), Sweden (Lindström and Erlström, 2006), Germany (Heunisch et al., 2010), England (Bonis et al., 2010), Hungary (Götz et al., 2009), and Austria (Bonis et al., 2009) show simultaneous changes in floral assemblages over a very broad area. Early Rhaetian vegetation in NW Europe consisted of a diverse community of pollen-producing gymnospermous trees and shrubs, including seed ferns, cycads, ginkgophytes, gnetaleans, bennettitaleans, and conifers with an understory of ferns and fern allies (mosses, horsetails, lycopsids). Palynological assemblages from the uppermost Rhaetian Triletes Beds in Germany, and equivalent beds in Denmark and Sweden, show a strong decline in tree pollen abundance and a surge in fern spores dominated by *Polypodiisporites polymicroforatus* and various morphotypes of the *Deltoidospora-Concavisporites* complex. Across NW Europe the predominantly arborescent (tree-dominated) flora was replaced during the latest Rhaetian by a pioneer vegetation consisting of ferns and fern allies, being dominated by only a few groups of ground ferns (van de Schootbrugge et al., 2009). Taken together these observations suggest that deforestation during the end-Triassic extinction was a key factor in driving ecosystem change.

Here, we use palynological data for the end-Triassic mass-extinction event (ETME; 201.6 Ma) from four different cores from Denmark (Stenlille), France (Boust), and Germany (Schandelah and Mingolsheim) as a proxy to examine intense soil erosion and bedrock weathering related to forest dieback across the Triassic-Jurassic boundary. In addition, we develop a new proxy-record for soil erosion based on the intensity of biological degradation of palynomorphs by soil-borne organisms. Our long-term palynological records allow us to also trace the resilience of soils following the end-Triassic extinction.

2. Material and methods

2.1. Material

The presented work is based on new palynological analyses from the Schandelah-1 core (northern Germany) and Boust core (northern France), combined with previously published data from the Stenlille core (Denmark; Lindström et al., 2012) and Mingolsheim core (southern Germany; van de Schootbrugge et al., 2009). The four cores form a north to south transect and represent different basins within the European Epicontinental Seaway, with the Stenlille core representing the Danish Basin, the Schandelah-1 core representing the North German Basin, the Mingolsheim representing the South German Basin and the Boust core representing the Paris Basin (Fig. 1).

The Stenlille structure is a gentle anticline on top of a salt pillar. More than 20 wells were drilled through the T/J-transition encompassing the sandstone-dominated Gassum Formation and succeeding mudstone-dominated Fjerritslev Formation to assess the reservoir and cap rock quality, respectively, as the structure is used for storage of natural gas. The Stenlille-1 well was drilled in 1980 and cored over the T/J-transition. The litho-, bio-, and chemostratigraphy of the Stenlille succession in the Danish Basin has been presented in Nielsen (2003) and Lindström et al. (2012, 2015, 2017). The lower to middle Rhaetian Gassum Formation consists of interbedded fine- to medium-grained, occasionally coarse-grained and pebbly sandstones, heteroliths, mudstones and a few thin coaly beds, formed in a shallow marine to coastal environment. It is succeeded by the lowermost part of the Fjerritslev Formation which consists of dark grey shale. This shale unit was deposited during the late Rhaetian transgression and a regionally recognized maximum flooding surface (MFS 7 of Nielsen, 2003) is located in the middle of the ca. 3 m thick shale. Palynological assemblages of the Gassum Formation and the dark grey shale at the base of the Fjerritslev Formation are assigned to the *Granuloperculatipollis-Classopollis-Perinopollenites* (GCP) zone, which is dominated by conifer pollen, primarily the nominate taxa (Lindström, 2016). These pollen groups decrease in abundance upwards within the dark grey shale and are virtually absent in the succeeding zone. Dinoflagellate cysts also decrease dramatically in abundance and *Rhaetogonyaulax rhaetica* has its last common occurrence (LCO) in the middle of the dark grey shale.

The succeeding “grey siltstone” interval consists of greenish grey siltstones and fine-grained sandstones. Here, primary bedding features are undisturbed by bioturbation, allowing for the observation of multiple levels of soft-sediment deformations structures, seismites, which can be correlated with similar disturbed intervals across Europe (Lindström et al., 2015). The seismites are interbedded by intervals of undisturbed strata. Wave-ripple cross-lamination indicates deposition at depths above storm wave base (Lindström et al., 2015). The lower c. 3 m of the “grey siltstone” interval contains abundant clay clasts (Lindström et al., 2017). The palynoflora from the grey siltstone interval belongs to the *Polypodiisporites-Ricciisporites-Deltoidospora* (PRD) zone, which differs significantly from the previous zone. This zone correlates with the *Ricciisporites-Polypodiisporites* Zone of Lund (1977) and is dominated by *Polypodiisporites polymicroforatus, Ricciisporites tuberculatus* and *Deltoidospora* spp., while conifer pollen are virtually absent (Lindström, 2016). *Ricciisporites tuberculatus* is common to

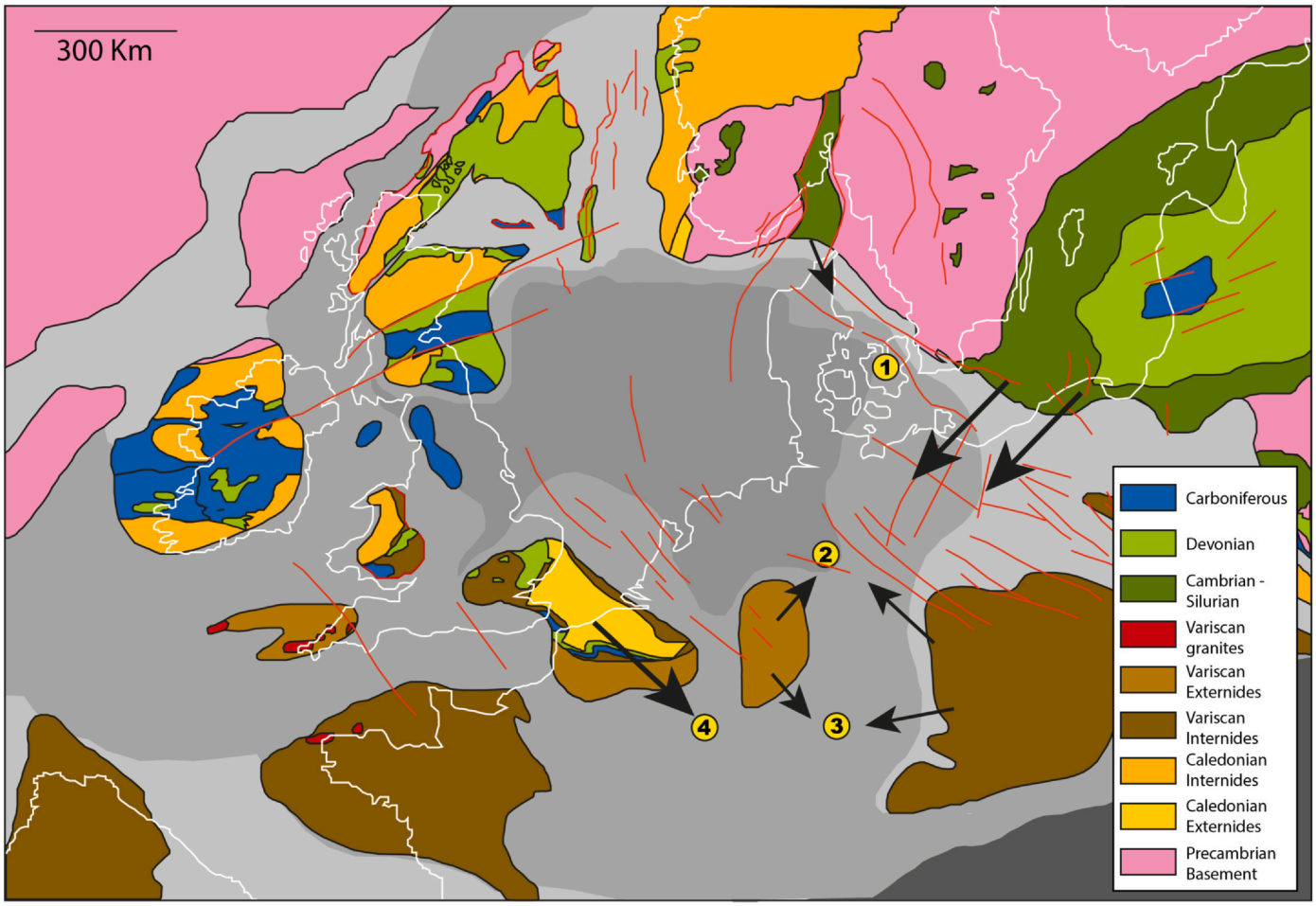

Fig. 1. Geological base map and location map for the Triassic-Jurassic transition in NW Europe. This reconstruction is based on combining two maps originally published by Ziegler (1990). The reconstruction uses the Permian base map as an overlay on the Jurassic palaeogeographic marine facies map. The arrows indicate directions of reworking and probable source areas. (1) Stenlille, Demark. (2) Schandelah, Germany. (3) Mingolsheim, Germany. (4) Boust, France.

abundant in the GCP zone and remains relatively abundant throughout the grey siltstone interval (Lindström, 2016). High levels of *Polypodiisporites polymicroforatus,* are restricted to the PRD zone after which it decreases markedly. *Cerebropollenites thiergartii* is first recorded in the uppermost part of the interval (Lindström et al., 2017).

The grey siltstone is followed by marine claystones, mudstones and fine-grained sand intervals, deposited during another transgressive event. The palynofloras are interpreted to reflect floral recovery, and are assigned to the *Calamospora-Conbaculatisporites-Monosulcites* (CCM) and *Perinopollenites-Deltoidospora-Stereisporites* (PDS) zones (Lindström, 2016). *Kraeuselisporites reissingerii* and *Ischyosporites variegatus* have their FOs in the lowermost part of the PDS zone, and in its upper part the dinoflagellate cyst *R. rhaetica* occurs for the last time. The FCO of *Pinuspollenites minimus* marks the lower boundary of the *Deltoidospora-Perinopollenites-Pinuspollenites* (DPPi) zone, which is dominated by *Deltoidospora* spp., *Perinopollenites elatoides* and *P. minimus.* Lindström (2016) correlated the DPPi zone and the succeeding *Perinopollenites-Pinuspollenites* (PPi) zone with the *Pinuspollenites-Trachysporites* Zone of Lund (1977), and placed these zones within the post-extinction phase.

The Schandelah-1 core was drilled close to the town of Braunschweig in northern Germany and detailed bio-, chemo-, and lithostratigraphy can be found in van de Schootbrugge et al. (2019). The upper Rhaetian (338.00–318.60 mbs) Exter Formation includes the 'Contorta Beds' (334.80–332.00 mbs) and the overlying 'Triletes Beds' (332.00–318.60 mbs). The former consists of current-rippled sandstones with intercalations of thin mud beds. Charcoal and plant material are abundant in this unit. The 'Triletes Beds' consists of grey to dark grey sand- and siltstones characterized by pronounced and varied sedimentary structures. Liquefaction horizons, described as seismites in Lindström et al. (2015), are common in this interval. Mud-chip conglomerate beds occur throughout the Triletes Beds, with clasts typically highly rounded and up to 1 cm in diameter. Also, sandstone beds with cross-stratification include climbing ripples, suggesting high sediment influx. Although fossils are largely absent, there is evidence of bioturbation between 330.35 and 330.00 mbs. The Rhaetian-Hettangian boundary is placed at a sharp surface (318.6 mbs) at the base of a 70 cm thick shale which lies within a bioturbated sandstone unit characterized by increasingly better developed laminations towards the top. The Hettangian (318.60–233.30 mbs) consists of a heterolithic succession of alternating silt- and sandstone lenses interspersed with organic-rich mudstones and shales, typical of mudflats under tidal influences. Gutter casts are common. Several intervals contain thick sandstone beds that are recognized as regional marker beds. The lower part of the Hettangian from 318.00 to 298.00 consists of laminated dark-grey mudstones with intervals that contain paper shales. Macrofossil content is of low abundance throughout the Hettangian, with the exception of trace fossils, crinoid remains, and sparse ammonite remains. Noticeable intervals contain the gradual transition into distinctly red-coloured laminated claystones at 258.65–254.80 mbs and 238.00–234.00 mbs. Apart from the colour, the lithology is not strikingly different from under- and overlying dark-grey laminated shales. It remains unclear whether these colour changes are primary or whether they are diagenetic in origin.

The Mingolsheim core was drilled in 1968 (Hettich, 1974; von

Hildebrandt and Schweizer, 1992) in the vicinity of Bad Mingolsheim, renamed Bad Schönborn in 1971 (Baden-Württemberg, Southern Germany). The litho,- bio-, and chemostratigraphic framework for the Mingolsheim core, including trace element and bulk organic carbon isotopes, was presented by Quan et al. (2008) and van de Schootbrugge et al. (2009). The sampled succession starts with the coarse grained continental 'Rhätsandstein', a massive sandstone that contains abundant plant remains. This is overlain by the Contorta Beds, black shales rich in marine dinoflagellate cysts, such as *Rhaetogonyaulax rhaetica*, a marker species for the Rhaetian. The Contorta Beds are overlain by 7 m of uniform grey claystones known as the Triletes Beds of latest Rhaetian age. These claystones are devoid of any macrofossil remains. The transition to the Jurassic is marked by an indurated sandy limestone bed known as the Psilonoten Limestone, named after the first occurrence of Jurassic psiloceratid ammonites. The lowermost part of the Hettangian appears to be either missing or is highly condensed in the Mingolsheim core. The Hettangian and base of the Sinemurian in the Mingolsheim core consist of organic rich shales. Compared to other successions in this report, the Hettangian is extremely condensed, suggesting deposition in deeper marine conditions.

The Boust core was drilled in 1986 close to the Hettangian stratotype in Grande Hettange, northeastern Lorraine, near the Luxembourg and German borders. The investigated and sampled part of the core measures 37.30 m from 69.90 m below surface (mbs) in the uppermost Norian to 32.20 mbs in the Hettangian. The Rhaetian sequence ranges from 67.00 m to 38.81 m, representing by far the thickest and most complete Rhaetian from all cores analyzed recently in the northeastern Paris Basin (Kuhlmann, 2019). The uppermost Norian ('Steinmergelkeuper') consists generally of light greenish-grey dolomitic marls. It is truncated by a thin conglomerate, an indicator of the Rhaetian transgression that is found in all drillcores in the northeastern Paris Basin. This is overlain by the *Contorta Beds* of the lower Rhaetian up to 47.16 m, representing in northern Lorraine the facies of the so called "Sables de Mortinsart". Its lower part consists of exceptionally thick laminated silty clay, with lenses and layers of silt. From 57.00 to 55.00 m the proper Sables de Mortinsart occurs. It forms the top of a sandy coarsening-up cycle that ends with conglomeratic layers with evidence for desiccation. Above 50.80 m clay reappears. Its planar lamination is perturbed by convolute structures of soft sediment deformation (seismites). The lower Rhaetian ends with some irregular conglomerate beds with intercalated, microfolded layers of silty clays, topped by structureless grey clay with *Rhaetavicula contorta* and *Isocyprina* sp. This sequence has been suggested to represent tsunami deposits triggered by the Rochechouart impact, which can be recognized in the end-Triassic sediment archive throughout the Paris Basin (Kuhlmann, 2019). A rapid change to thick, reddish-brown clays starts at a depth of 45.16 m. They reach up to 38.81 m and represent the upper Rhaetian, stratigraphically belonging to the 'Argiles de Levallois'. Near 45.00 m a microfolded slumping horizon (seismite) can be observed. The clays grade sharply into the dark grey, bioturbated marls of the lower Hettangian ('Psiloceras beds') with intercalated biodetritic limestone beds in the lower part. The typical ammonite *Psiloceras planorbis* was found at 36.23 m. At the top of the section (32.20 m) more frequent occurrence of plant debris is observed. A detailed sedimentological, geochemical and mineralogical description of Boust and other sections of the northeastern Paris Basin is presented in detail in Kuhlmann (2019).

2.2. Palynology

A description of sample preparation methods used for Mingolsheim and Stenlille is provided in van de Schootbrugge et al. (2009) and Lindström et al. (2012), respectively. The drillcore Boust was described and sampled by N. Kuhlmann and J. Thein at the University of Lorraine in Nancy (France). Samples from the Schandelah-1 and Boust cores were processed at Utrecht University. Approximately 10 g of freeze dried sample was crushed to ~1–3 mm^3 fragments. Carbonates and silicates were removed by washing the samples twice with 30% HCl and 40% HF. Where needed, oxidative maceration was performed with by $KClO_3$ and 65% HNO_3 to remove the bulk of the amorphous organic matter. After neutralizing, the samples were sieved over a 250 μm mesh to remove coarse material and subsequently over a 10 μm mesh to remove the finest, amorphous material. The heavy mineral fraction was removed from the lighter organic fraction by bringing the light fraction in suspension in an ultrasonic tub. The remaining light fraction was mounted on glass microscopic slides with glycerin jelly. The surplus material was collected in a small glass vial and is stored at the Department of Earth Sciences, Utrecht University for future reference. Samples were analyzed under 1000× magnification with an optical microscope (Leica) and relative abundances were determined by counting approximately 300 palynomorphs per slide. A subset of samples was spiked with *Lycopodium* and these were counted quantitatively.

2.3. Biodegradation

There is no single method for quantifying palynomorph preservation and none tailored for geological deep time. Therefore, the methodologies we use here are based on a pollen preservation system developed for Quaternary sporomorphs (Havinga, 1967). Typically 5 classes of degradation are distinguished: (1) corrosion, (2) degradation, (3) crumpling, (4) physical damage, and (5) intact preservation (Havinga, 1967; Twiddle and Bunting, 2010). As the aim of this study was to quantify biodegradation across the Rhaetian-Hettangian boundary, the focus was solely on corrosion. The other categories are related to transport as opposed to biological degradation in soils. Corrosion of palynomorphs is described as etching or pitting of the exines, whereby the circular to rectangular holes often with scalloped edges are randomly scattered on the surface of the sporomorphs. Generally, this form of corrosion only affects the ektexine, the outer layer of the wall of the sporomorph grains. In extreme cases, however, the ektexine may be almost completely eaten away, or leaving only fragments of the ektexine on the intact endexine (Cushing, 1967). Corrosion also includes deterioration a material undergoes as a result of its interaction with its surroundings, including physical, chemical or biological processes. Microbial attack is one of the more important biological processes grouped in this class (Havinga, 1967). Specific, repetitive patterns of corrosion shown on pollen, spores and other plant debris, can be of fungal or bacterial origin (Goldstein, 1960), but it is the primitive fungal group, the chytridiomycetes ("chytrids"), that are the most well-know pollen pathogens today. These saprophagous microfungi penetrate the pollen wall and consume the cell contents of pollen floating in lakes or retained in soils (Skvarla and Anderegg, 1972; Czeczuga and Muszynska, 2001). Chytrids, which first occur in the Devonian Rhynie Chert, have a long association with soil ecosystems throughout the geological record of terrestrial deposits.

For the purpose of this study, the broadly defined category "corrosion" was split into two subcategories: (1) corrosion as a result of the physical and chemical alteration of the sporomorphs. (2) biodegradation due the activity of micro-organisms. We quantified the level of corrosion attributable to micro-organisms using only smooth, trilete fern spores belonging to *Deltoidospora* and *Concavisporites* (*Concavisporites-Deltoidospora*-complex; Fig. 2). These genera were chosen as proxy taxa because of their high abundance and continuous occurrence from the Rhaetian to upper Hettangian. Furthermore, these taxa are characteristic for the fern peaks during the Late Triassic – Early Jurassic in the Schandelah-1 core. Fluctuations in abundance of *Concavisporites-Deltoidospora* led to the exclusion of ~30 samples in which a minimum of 50 specimens per sample could not be attained. In samples with abundant proxy taxa, counts are based on 100 specimens of trilete spores. A distinction was made between differing levels of biodegradation observed in each specimen. We partitioned these degrees of

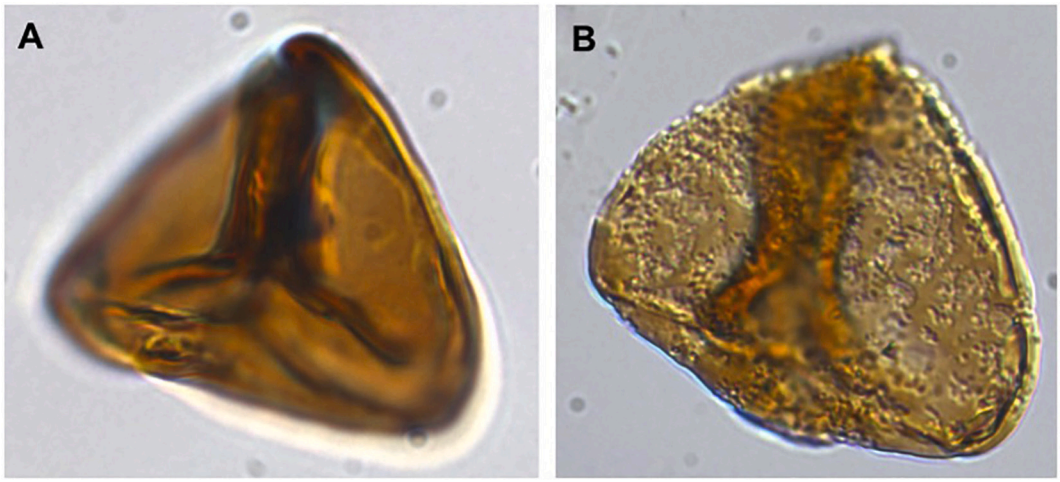

Fig. 2. Examples of Triassic-Jurassic smooth trilete spores of the *Concavisporites-Deltoidospora* complex. The specimens show an increase in the degree of biodegradation from (a) no biodegradation to (b) severe biodegradation of the spore wall.

biodegradation into three classes: (1) none – minor pitting, (2) high amount of pitting and/or etching but no distinct biological pattern, (3) distinct biological patterns. In total, 91 slides were counted over the depth interval 228–338 mbs, spanning the Rhaetian to lowermost Sinemurian.

3. Results

3.1. Reworking and vegetation change

In all four cores the loss of four of the most common taxa of late Triassic pollen, *Ovalipollis ovalis, Lunatisporites rhaeticus, Rhaetipollis germanicus,* and *Ricciisporites tuberculatus* occurs during the latest Rhaetian (Fig. 3), reaching a nadir at the Triassic-Jurassic boundary. These four pollen taxa, representing a diverse mix of gymnospermous plants, including cycads, conifers, and peltasperms, make up on average 30 to 50% of the total palynomorph fraction. A particularly prominent victim of the end-Triassic extinction was the enigmatic gymnospermous pollen taxon *Ricciisporites tuberculatus* (Mander et al., 2012a). In the Schandelah-1 core, *R. tuberculatus* gradually decreases in abundance and finally disappears at 318.65 mbs around the Triassic-Jurassic boundary. The extinction of *R. tuberculatus* is part of a general trend towards an assemblage that is nearly devoid of tree-pollen, differing starkly from underlying Rhaetian and overlying Hettangian assemblages (compare for example van Eldijk et al. (2018) for a plot of long-term trends in pollen taxa). The step-wise disappearance and eventual extinction of these four taxa can be observed in all four areas (Fig. 3), although spikes in abundance in the Stenlille core are somewhat obscuring this trend.

In all four cores the loss of pollen is accompanied by substantial

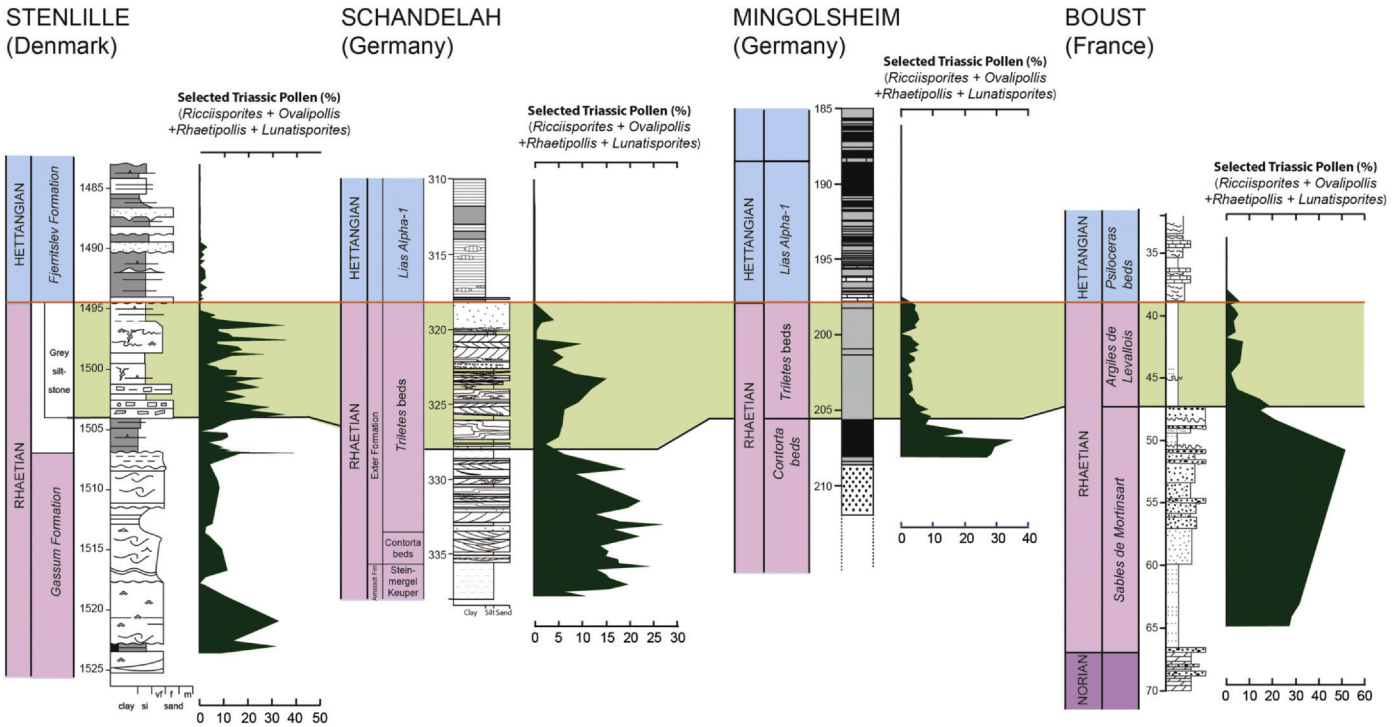

Fig. 3. Correlation of pollen abundance for the four investigated cores. Plotted here is the sum of the "big four" Triassic taxa that go extinct at the Triassic-Jurassic boundary, including *Ovalipollis ovalis, Rhaetipollis germanicus, Lunatisporites rhaeticus*, and *Ricciisporites tuberculatus*.

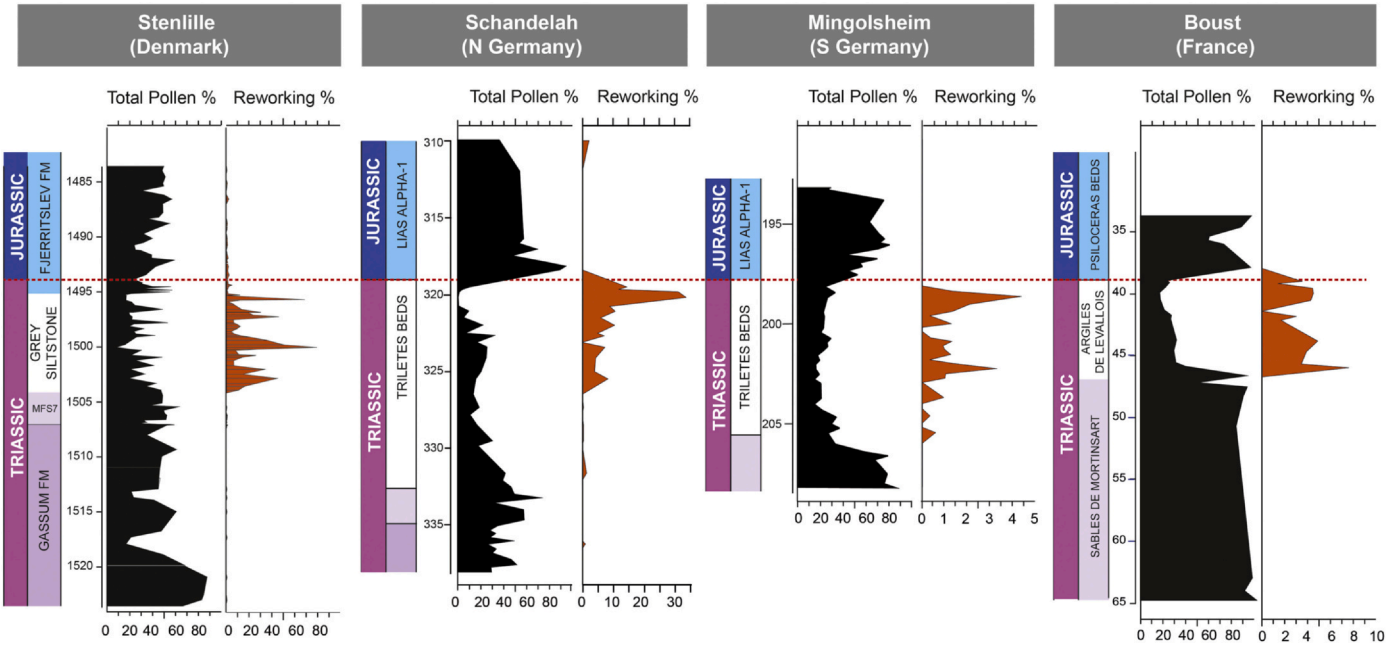

Fig. 4. Palynological diagram showing total pollen abundance and reworking as a percentage of the total fraction. Reworking strongly increases within the Triletes Beds in Germany and in correlatable units in Denmark and France.

increases in fern spore abundance together with increases in bryophyte spores and spores from horsetails. For the Germanic and Danish Basins, these data have been discussed extensively in a set of papers on fern proliferation during the end-Triassic extinction (Lindström et al., 2012, Lindström, 2016; van de Schootbrugge et al., 2009, 2019; Barth et al., 2018a;). Here, we focus on the link between pollen loss indicating deforestation, and the reworking of palynomorphs.

All four studied cores provide a consistent record of reworking of palynomorphs that is highly correlated with the main phase of deforestation (Fig. 4) within the Triletes Beds in Germany, and its equivalents in Denmark ('grey siltstone' interval) and France ('Argiles de Levallois'). In the Schandelah-1 core, the exact same interval within the upper part of the Triletes Beds that contains evidence for forest dieback, also contains a remarkable and unusual record of abundant reworked Palaeozoic palynomorphs. Within the top part of the Triletes Beds (327.00 to 318.80 mbs) large quantities of Palaeozoic acritarchs and prasinophyte cysts (phycomata) were encountered (Figs. 4, 5 and 6) comprising up to 35% of the total palynomorph assemblage. In several samples around 321.00 mbs, reworked acritarchs/prasinophytes constitute the second-most dominant palynomorph group. Prasinophyte phycomata (e.g. *Tasmanites* and leiosphaerids) are mostly long-ranging undiagnostic taxa, and many are poorly preserved. In contrast, the quality of preservation of the acritarch specimens is exceptional (Figs. 5, 6), enabling species-level taxonomic identifications. The identified acritarchs are exclusively Silurian and Ordovician in age (Table 1). Except for *Acanthodiacrodium ubui*, and some *Polygonium* and *Baltisphaeridium* species, all of the encountered acritarch specimens are singletons (Table 1). This pattern of recovery is typical of reworked assemblages. Overall, 20 different Palaeozoic acritarch species were recognized.

Reworking reached a climax just before the Triassic-Jurassic boundary in the Schandelah-1 core and declined sharply into the Hettangian. However, reworking did continue at low levels for much of the Hettangian (Fig. 7). In addition to minor occurrences of additional Palaeozoic acritarchs, reworking during the Hettangian is mainly characterized by reworking of Triassic palynomorphs, marked by single occurrences of *Ovalipollis* and *Ricciisporites*. There are two two red shale intervals within the upper Hettangian Angulata Zone (Fig. 7) that show increased numbers of reworked palynomorphs, including numerous examples of *Aulisporites astigmosus*, signaling reworking of Middle-Upper Triassic (upper Ladinian to Carnian) sediments.

Both red shale intervals are characterized by declines in both relative and absolute pollen abundance (Fig. 7), although the absolute quantitative data set is somewhat patchy due to low counts of *Lycopodium* in several samples. Minima in pollen total abundance are predominantly related to decreased abundance of *Classopollis* and *Perinopollenites*. Their relative decline is compensated by increases in fern spores of the *Concavisporites-Deltoidospora* complex. Reworking appears to have ceased at the Hettangian-Sinemurian boundary, however, the reworking signal could possibly be masked by a very pronounced increase in pollen abundance (Fig. 7), mainly of *Perinopollenites elatoides*. The Sinemurian shows a dominance of tree pollen and very reduced numbers of spores overall.

In the Mingolsheim core (Fig. 8) the Triletes Beds contain numerous specimens of reworked *Veryhachium* and several specimens of *Multiplicisphaeridium,* together with a suite of other unidentified Palaeozoic acritarchs and prasinophytes. Perhaps, much more significant is an abundance of peculiar palynomorphs that bear similarity to Neoproterozoic palynomorph assemblages known from localities worldwide. These reworked palynomorphs share a common grey-brown preserved appearance that is distinctly different from authochthonous material and also differs from reworked Palaeozoic acritarchs. The genus *Germinosphaera* (Fig. 8a–c) is present in multiple samples from the Triletes Beds, occurring together with undetermined acanthomorph acritarchs (Fig. 8d–e). *Germinosphaera* has recently been recovered from the Shaler Group of Meso- to Neoproterozoic age (Loron et al., 2019), but it has a very wide distribution and also occurs in the Tonian of the East European Platform in Russia (Vorob'eva et al., 2009). *Ostiana microcystis* is present in sample MING-39 (Fig. 8f). In addition, we find many differently shaped palynomorphs that are reminiscent of the Neoproterozoic form taxon *Jacutianemia solubila* (Fig. 8i, h and k) as recently described from the Tonian of North China (Li et al., 2019), but also present in the East European Platform (Vorob'eva et al., 2009). We also find numerous distinctly branched tubes (Fig. 8g) in different samples, which resemble the recently described Neoproterozoic form genus *Ouraisphaera giraldae* (Loron et al., 2019). Also present are coiled flattened filaments (Fig. 8j) that can be assigned to *Obruchevella,* a presumed filamentous cyanobacteria that has been reported from the

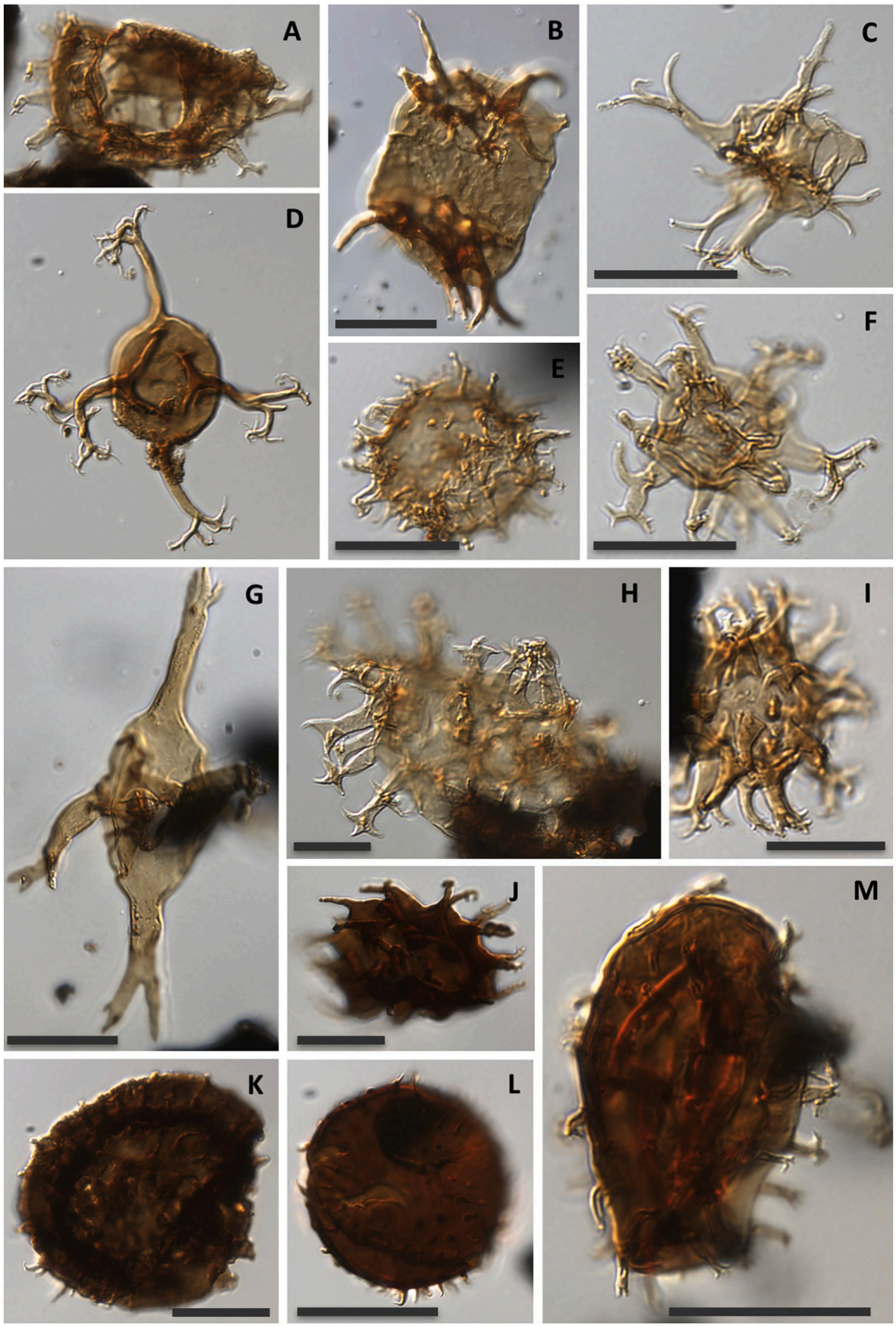

(caption on next page)

Fig. 5. Identified Ordovician and Silurian acritarchs from the Triassic-Jurassic boundary interval in the Schandelah core (see also Table 1). Scale bars are 20 μm. **(a)** *Cymatiogalea* cf. *C. deunfii* - Sample Sch 324.10. **(b)** *Acanthodiacrodium* sp. - Sample Sch 324.10. **(c)** *Multiplicisphaeridium* sp. - Sample 322.70. **(d)** *Oppilatala eoplanktonica* - Sample Sch 322.70. **(e)** *Ammonidium* cf. *A. microcladum* - Sample Sch 323.40. **(f)** *Multiplicisphaeridium* sp. - Sample Sch 322.50. **(g)** *Evittia* sp. - Sample Sch 322.70. **(h)** *Ankyrotrochus crispum* - Sample Sch 322.50. **(i)** *Multiplicisphaeridium* cf. *M. raspa* - Sample Sch 320.20. **(j)** *Stellechinatum* cf. *S. uncinatum* - Sample Sch 321.10. **(k)** *Baltisphaeridium* cf. *B. dasos* - Sample Sch 321.10. **(l)** *Baltisphaeridium* cf. *B. dasos* - Sample Sch 320.20. **(m)** *Stelliferidium* sp. - Sample Sch 320.20.

Neoproterozoic of the East European Platform by Vorob'eva et al. (2009) and elsewhere, including the Doushanto. Taken together there is clear evidence for abundantly reworked Neoproterozoic organic-walled palynomorphs in the Triletes Beds in the Mingolsheim core.

In the Boust core (Fig. 9) reworking increases dramatically within the latest Rhaetian Argiles de Levallois, which is the Paris Basin equivalent to the Triletes Beds in Germany. Reworked palynomorphs are mostly comprised of Carboniferous spores that stand out from authochtonous spores by being darker and generally more poorly preserved. Also undetermined Palaeozoic acritarchs and prasinophyte phycomata are present although they are less abundant than in Schandelah-1. We note the presence of spores assignable to *Lycospora, Spencerisporites,* and *Cingulizonates*, all of which have a late Carboniferous age. Some of these taxa have in the past been incorporated in quantitative analyses of Rhaetian floras, which suggests that there could be a serious problem with vegetation reconstructions.

In the Stenlille cores (Fig. 9), reworked early Palaeozoic, Carboniferous and Middle to Late Triassic palynomorphs (up to 10% of the total fraction) are common within the latest Rhaetian "grey siltstone" interval of the Fjerritslev Formation (Lindström et al., 2012). Lower Palaeozoic (Ordovician–Silurian) reworked palynomorphs include *Evittia denticulata*, *Nexosarium leherrisei, Oppilatala* sp., *Cymbosphaeridium* sp., *Multiplicisphaeridium* spp. and *Neoveryhachium carminae*. The cryptospore *Tetrahedraletes medinensis* is also found reworked within this interval. It is known from Upper Silurian to Lower Devonian strata in Scania in southern Sweden (Mehlqvist et al., 2015). A single specimen of *Emphanisporites micrornatus* present in the "grey siltstone" interval in the Stenlille-4 core, also occurs in the Lower Devonian (Lockhovian) of Scania (Mehlqvist et al., 2015). Reworked Carboniferous spores and pollen include *Cingulizonates* spp., *Crassispora kosankei, Densosporites* spp., *Lycospora pusilla, Florinites* sp., *Schulzospora rara* and *Tripartites vetustus,* derived from Visean and Namurian to Westphalian palynofloras (Clayton et al., 1977). Carboniferous spores and pollen have previously been encountered in Jurassic and Cretaceous strata of southern Sweden and the Danish island of Bornholm (Nielsen and Koppelhus, 1991; Lindström et al., 2017). Late Middle to Late Triassic pollen are also encountered, including *Retisulcites perforates, Echinitosporites iliacoides, Staurosaccites quadrifidus, Illinites chitonoides, Protodiploxypinus gracilis* and *Striatoabieites* spp. Several of these Silurian to mid-Triassic taxa have also been found reworked within the "grey siltstone" in southern Sweden, along with rare chitinozoans (Lindström et al., 2017). Although initially not considered to be reworked, abundant sphaeromorphs (Fig. 9), likely representing the vegetative cysts of prasinophyte algae, may constitute up to 50% of the total palynomorph assemblage in some beds (Lindström et al., 2012). These sphaeromorphs vary significantly in appearance within a sample, both in colour and preservation, which may be explained by reworking from the Lower Palaeozoic along the Sorgenfrei-Tornquist Zone. In Scania (southern Sweden) the Lower Palaeozoic is intruded by numerous dykes of Carboniferous–Permian age. These dykes caused significant contact metamorphism in aureoles around the intrusives (Olsson-Borell and Ahlberg, 2003) and may explain the variations in colour observed in the sphaeromorphs and associated prasinophycean phycomata.

3.2. Corrosion of palynomorphs

In the Schandelah core, the biodegradation record (Fig. 7) is based solely on the percentage of smooth trilete spores showing clear biological patterns. Only a few spore specimens contain pitting marks related to chemical or physical corrosion as compared to percentages of the observed biodegradation pattern. Throughout the studied interval values of pitting vary between 0 and 30% and no clear pattern or trend is evident (not shown). For the entire interval, the mean percentage of pitting is 6.8%. Also, despite a few exceptions, the majority of the samples (~80%) show less than 10% pitting.

In the upper Rhaetian (318.6–338.0 mbs) biodegradation levels are low with a mean of ~26.4% (Fig. 7). Throughout the upper Rhaetian to the Hettangian-Sinemurian boundary the mean percentage of biological patterns of degradation on fern spores is 43.5%. A minimum of 8% biodegradation occurs in the uppermost Rhaetian, just before the boundary at 318.65 mbs. Across the Triassic-Jurassic boundary, at 318.6 mbs, the percentage of biodegraded fern spores increases sharply. A small drop occurs at 304.0 mbs of approximately 20%, which is coeval with the black and grey laminated mudstones in the lower Hettangian, just after the paper shales at a depth between 305.0 and 306.0 mbs. The number of spores with biological degradation patterns increases hereafter and values modestly fluctuate between ~45–85%. Following this steady increase, the biodegradation record rapidly decreases showing a sudden drop from 78% (259.0 mbs) to 26% (257.0 12 mbs). Low values of biodegradation continue to 254.0 mbs with only 16.7% biodegradation at this depth. This interval, 254.0–259.0 mbs, corresponds to the red-coloured laminated claystone deposited at 254.8–258.7 mbs. Hereafter, the amount of biodegraded spores rises again reaching a maximum value of 84% at 252.0 mbs. This high value is followed by a moderate low value of 31.5%, after which the biodegradation record fluctuates between approximately 32–51%. Following these relatively minor oscillations, two spikes show up in the record at 242.3 mbs and 240.0 mbs of 69.3% and 71.4%, respectively. This is followed by a second drop in the record that continues from 239.0 mbs to 234.0 mbs with biodegradation values between ~18–28%. This decline in the biodegradation record is coeval with the second red-coloured laminated claystone interval from 234.0–238.0 mbs. Next, towards the Hettangian – Sinemurian boundary (~230.2 mbs), the biodegradation values increase once more reaching 70% at 228.0 mbs. A minimum characterizes the Hettangian-Sinemurian boundary at 331.0 mbs (13.6%).

4. Discussion

4.1. Widespread soil erosion associated with the end-Triassic extinction

When exposed bedrock, in any terrain, contains organic-rich sedimentary rocks, those rocks may release palynomorphs as weathering and erosion take place. Such eroded and subsequently transported palynomorphs behave like silt-sized organic particles that are readily redeposited together with siliciclastic particles as sediments come to fill a depositional basin. Although the recognition of this reworked organic component presents a basic, but well-known challenge in stratigraphic palynology (Wilson, 1964), it is not a topic that is often addressed in the general literature, because, under normal conditions of sediment accumulation, the ratio of reworked to autochthonous palynomorphs is overwhelmingly diluted by input from contemporary material, and may become vanishingly small. Reworked components can be further diluted due to taphonomic loss during extended transport from more distant source areas, and, of course, much source bedrock itself (e.g. metamorphic and igneous rocks) does not act as a source of reworked palynomorphs at all. The recognition of reworking, therefore, becomes a potential tool for interpreting former sedimentary dynamics in ways

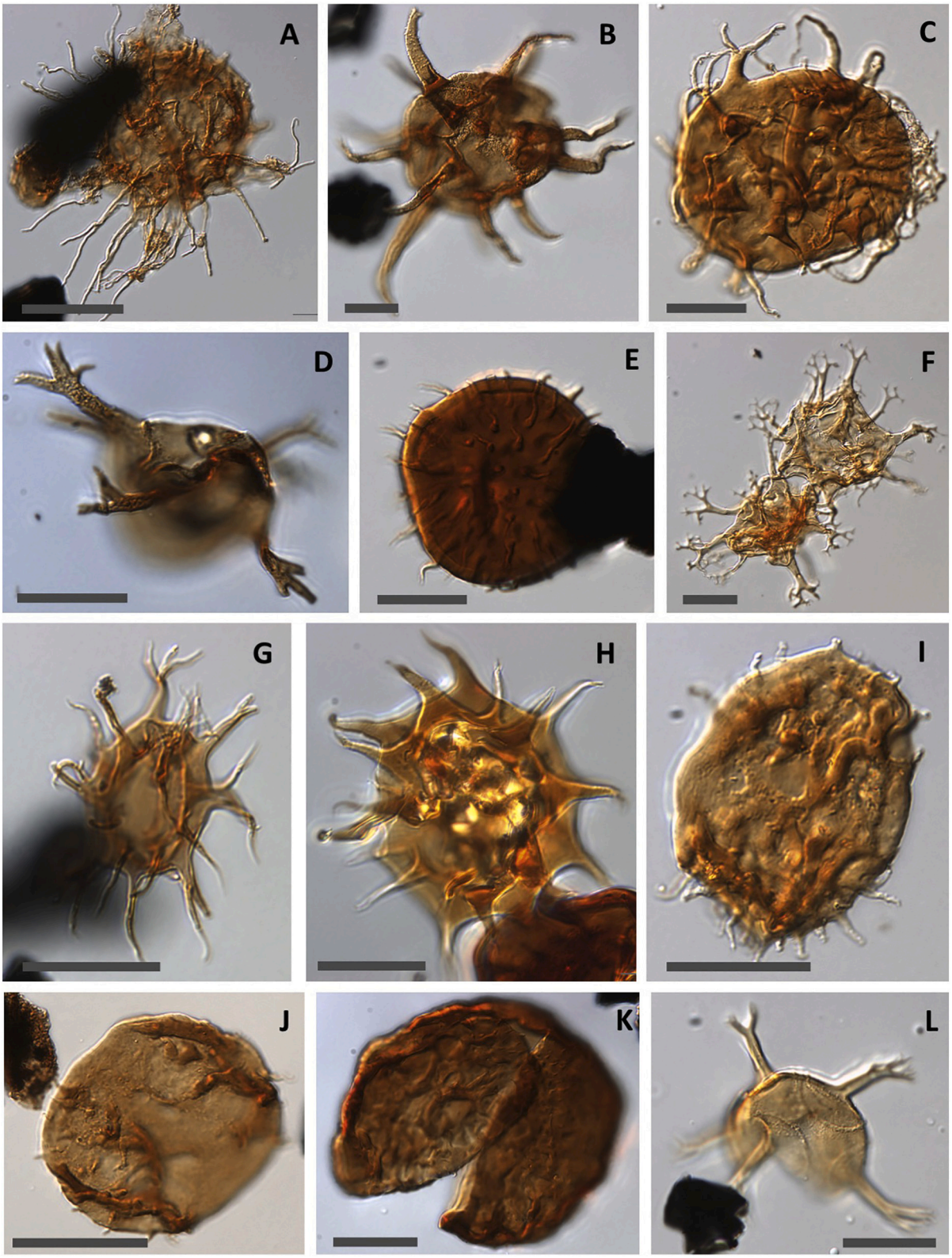

Fig. 6. Identified Ordovician and Silurian acritarchs from the Triassic-Jurassic boundary interval in the Schandelah core (see also Table 1). Scale bars are 20 μm. **(a)** *Elektroriskos* cf. *E. pogonius* - Sample Sch 320.20; **(b)** *Baltisphaeridium klabavense* - Sample Sch 320.20; **(c)** *Arbusculidium* cf. *A. ramusculosum* – Sample Sch 319.50; **(d)** *Evittia remota* - Sample Sch 320.20; **(e)** *Gorgonisphaeridium* sp. – Sample Sch 319.50; **(f)** *Vogtlandia* sp. - Sample Sch 319.50; **(g)** *Polygonium* cf. *P. fragilis* - Sample Sch 319.66; **(h)** *Polygonium* sp. – Sample Sch 319.66; **(i)** *Gorgonisphaeridium* sp. - Sample 319.50; **(j)** *Acanthodiacrodium ubui* – Sample Sch 319.66; **(k)** *Gorgonisphaeridium* sp. – Sample Sch 319.80; **(l)** *Cymbosphaeridium aniae* – Sample Sch 331.60.

Table 1
List of identified Ordovician and Silurian acritarchs reworked into the uppermost Rhaetian of the Schandelah-1 core together with their stratigraphic and absolute age range.

Depth (m)	Species	Age range	Stages	Top (Ma)	Base (Ma)	Average	Sample average	SD
319.5	*Arbusculidium* cf. *A. ramusculosum*	Lower Ordovician		471.80	488.30	480.05	461.62	17.3
319.5	*Gorgonisphaeridium sp.*	Upper Ordovician - Silurian		416.00	460.90	438.45		
319.5	*Vogllandia sp.*	Middle Ordovician		460.90	471.80	466.35		
319.66	*Polygonium* cf. *P. fragilis*	Middle Ordovician		460.90	471.80	466.35	468.39	10.0
319.66	*Polygonium spp.*	Ordovician		443.70	471.80	457.75		
319.66	*Polygonium spp.*	Ordovician		443.70	471.80	457.75		
319.66	*Acanthodiacrodium ubui*	Lower Ordovician		471.80	488.30	480.05		
319.66	*Acanthodiacrodium ubui*	Lower Ordovician		471.80	488.30	480.05		
319.80	*Ordovicidium heteromorphicum*	Middle - Upper Ordovician		471.80	443.70	457.75	457.75	14.1
320.20	*Baltisphaeridium* cf. *B. dasos*	Upper Ordovician		443.70	460.90	452.30	453.48	16.1
320.20	*Elektoriskos* cf. *E. pogonius*	Lower - Middle Silurian		426.20	443.70	434.95		
320.20	*Evittia remota*	Upper Ordovician		443.70	460.90	452.30		
320.20	*Stelliferidium sp.*	Lower Ordovician		471.80	488.30	480.05		
320.20	*Multiplicisphaeridium* cf. *M. raspa*	Lower - Middle Silurian		426.20	443.70	434.95		
320.20	*Baltisphaeridium klabavense*	Middle Ordovician		460.90	471.80	466.35		
320.80	*Acanthodiacrodium ubui*	Lower Ordovician		471.80	488.30	480.05	480.05	8.3
321.10	*Baltisphaeridium* cf. *B. dasos*	Upper Ordovician		443.70	460.90	452.30	463.45	11.2
321.10	*Stellechinatum* cf. *S. unctinatum*	Lower - Middle Ordovician		460.90	488.30	474.60		
322.50	*Multiplicisphaeridium sp.*	Middle Ordovician - Silurian		471.80	416.00	443.90	455.13	11.2
322.50	*Ankyrotrochus crispum*	Middle Ordovician		460.90	471.80	466.35		
322.70	*Evittia sp.*	Lower Silurian		443.70	428.70	436.20	438.77	3.6
322.70	*Multiplicisphaeridium sp.*	Middle Ordovician - Silurian		471.80	416.00	443.90		
322.70	*Oppilatala eoplanktonica*	Lower Silurian	Rhuddanian - Wenlock	443.70	428.70	436.20		
323.40	*Ammonidium* cf. *A. microcladum*	Middle Silurian	Wenlock	422.90	428.90	425.90	425.90	0.0
324.10	*Acanthodiacrodium sp.*	Lower Ordovician		471.80	488.30	480.05	480.50	0.0
324.10	*Cymatiogalea* cf. *C. deunfii*	Lower Ordovician	Tremadocian - Floian	471.80	488.30	480.05		
325.50	*Ordovicidium* cf. *O. elegantulum*	Upper Ordovician		443.70	460.90	452.30	452.30	0.0
331.6	*Cymbosphaeridium aniae*	Middle - Upper Silurian	Wenlock - Pridoli	428.90	416.00	422.45	422.45	0.0

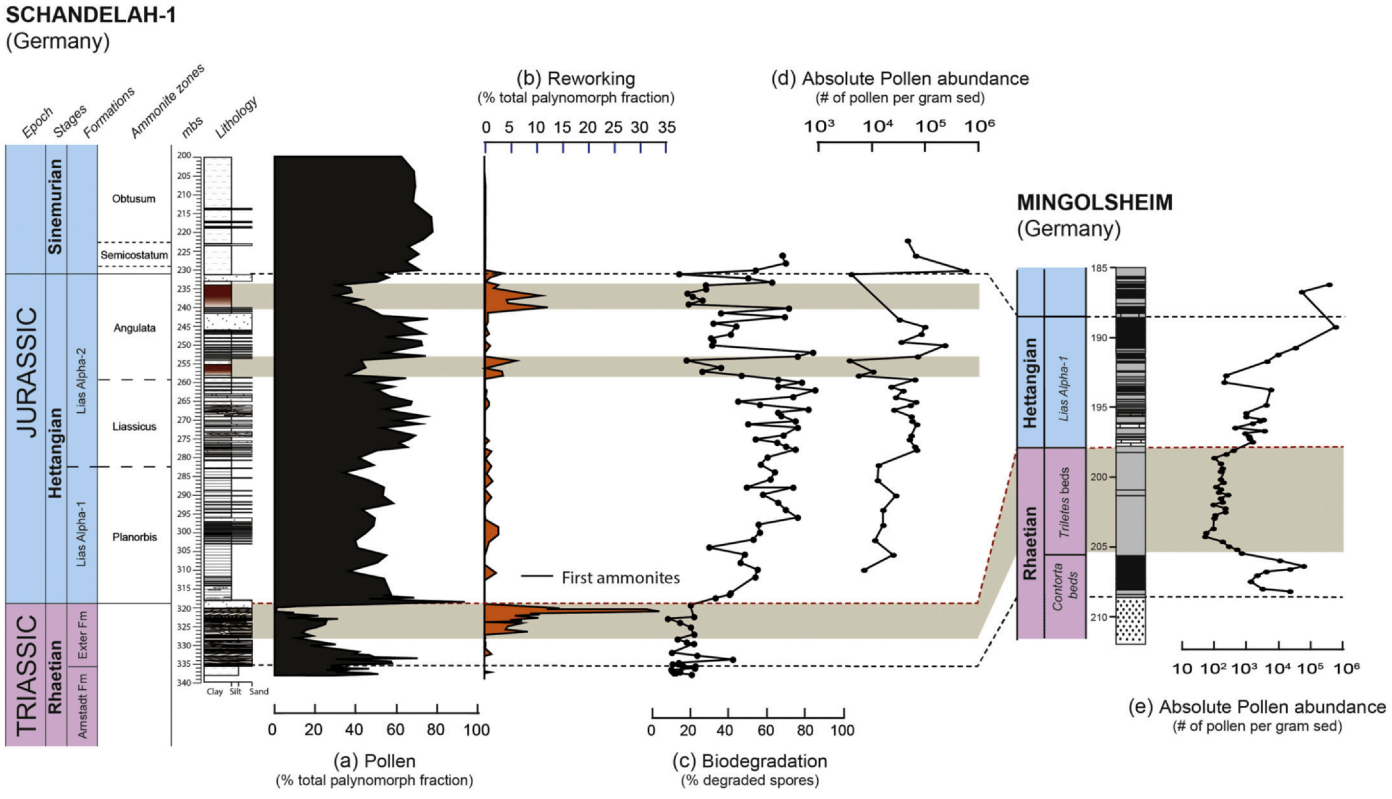

Fig. 7. Long term palynological records for the Schandelah-1 core. **(a)** Total pollen (% of total palynomorph fraction) showing clearly dramatic disappearance of pollen grains within the upper part of the Triletes Beds and declines associated with the red shale intervals. **(b)** Reworking as percentage of total palynomorph fraction. Both the Rhaetian and upper Hettangian show high numbers of reworked palynomorphs. **(c)** Biodegradation based on corrosion of 50 counted trilete spores per sample. **(d)** Absolute pollen abundance (pollen per gram sediment) showing decreased pollen abundance in red shale intervals. **(e)** Absolute pollen abundance (pollen per gram sediment) showing strong decline in absolute pollen abundance in the Triletes Beds marking deforestation during the end-Triassic mass-extinction. (For interpretation of the references to colour in this figure legend, the reader is referred to the web version of this article.)

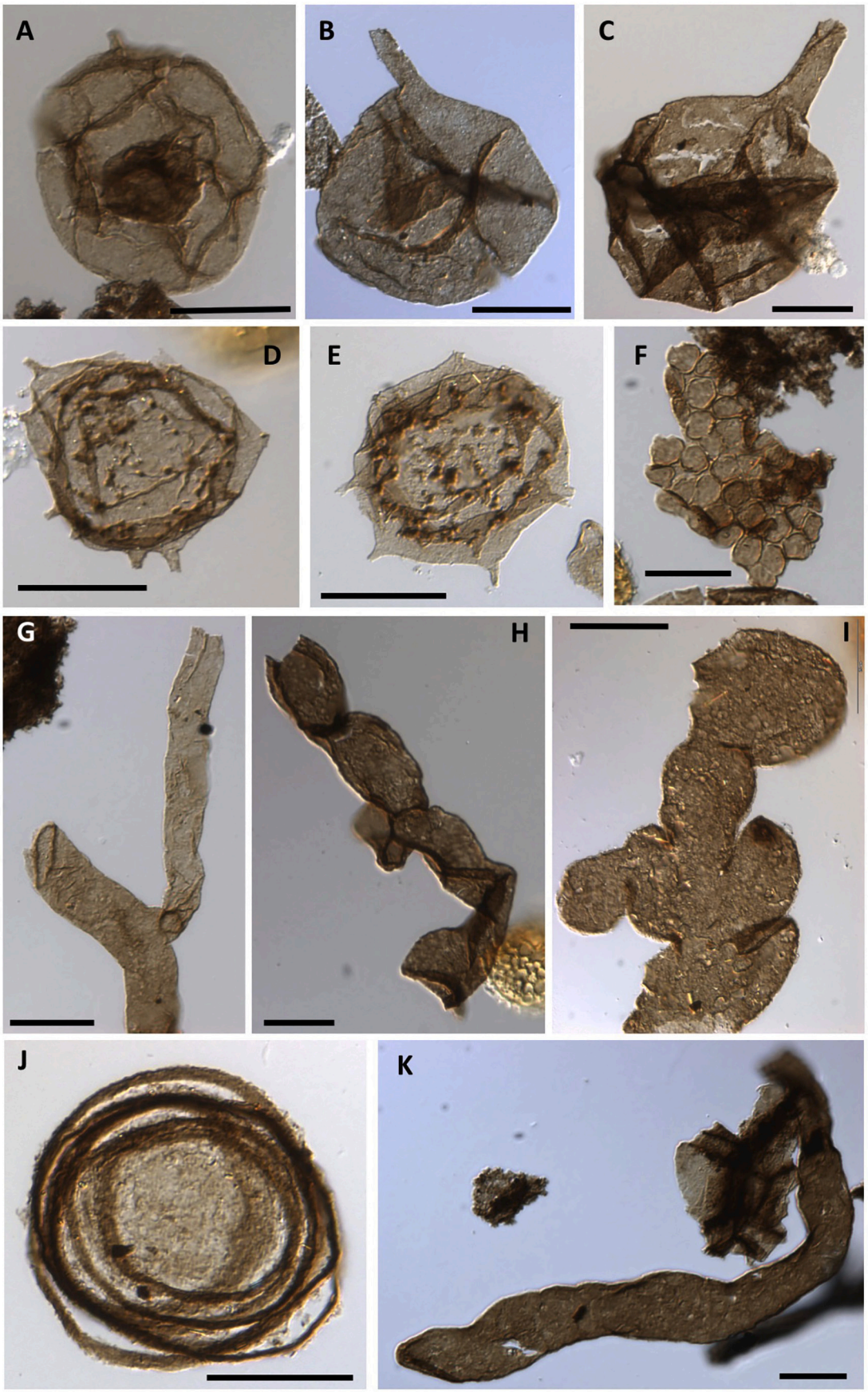

Fig. 8. Selected Neoproterozoic reworked palynomorphs from the Triassic-Jurassic boundary in the Mingolsheim core. All scale bars 20 μm. **(a-c)** *Germinosphaera* cf. *G. bispinosa*; **(d, e)** Undetermined acanthomorph acritarchs; **(f)** *Ostiania microcystis* Ming-39, Triletes Beds; **(g)** *Ouraisphaera giraldae;* **(h, i, k)** *Jakutianemia* spp.; **(j)** *Obruchevella valdaica*.

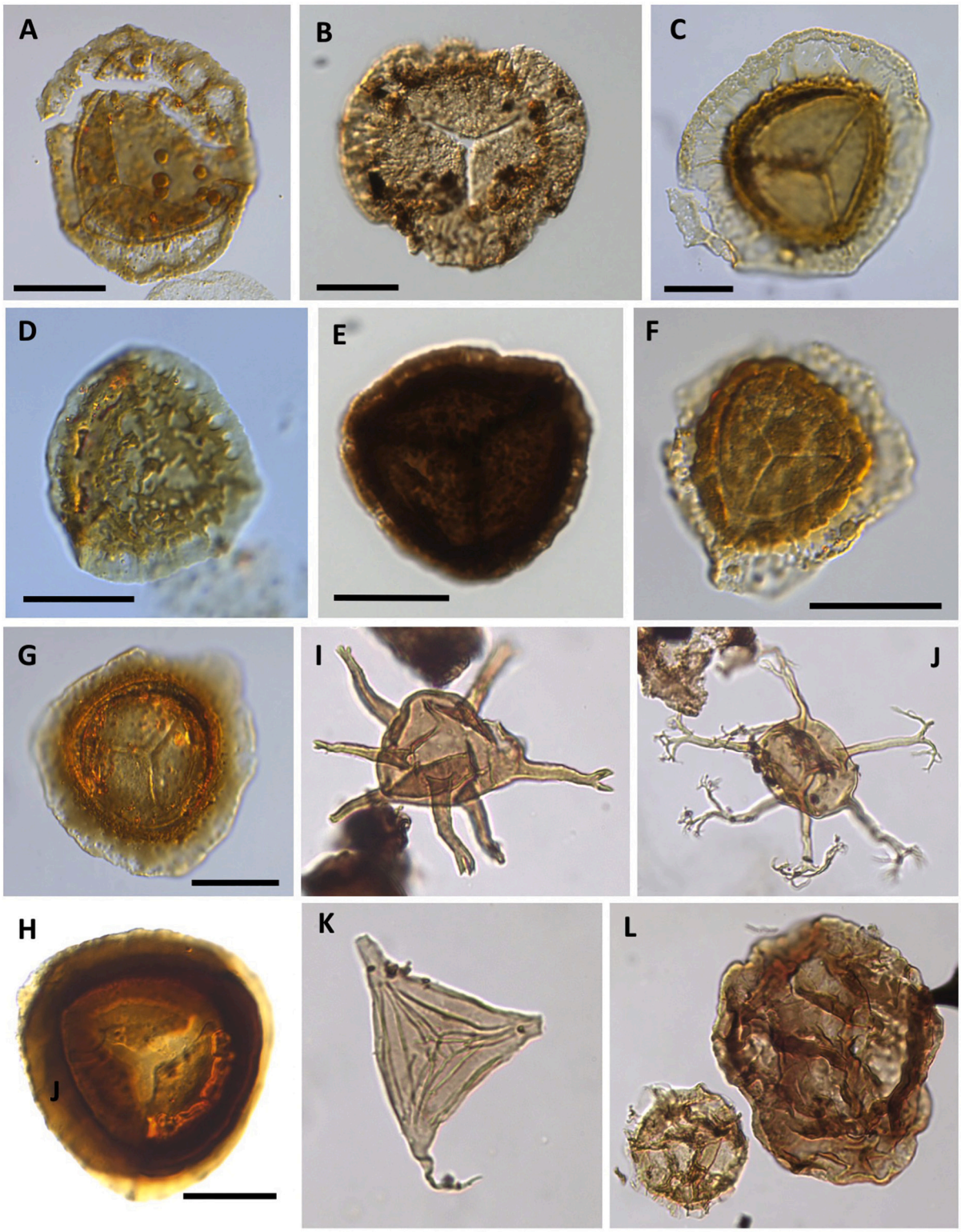

Fig. 9. Selected reworked palynomorphs from the Boust core (northern France) and Stenlille cores (Denmark). All scale bars 20 μm. **(a–h)** Reworked Carboniferous spores in the Boust core. **(i–l)** Reworked Palaeozoic acritarchs from Stenlille. **(a)** *Lycospora noctuina;* **(b)** *Spencerisporites spp.;* **(d–h)**: *Lycospora – Cingulizonates*.; **(i)** *Multiplicisphaeridium* sp. (cf. *Circinatisphaera aenigma*) Stenlille-4, 1508.83 m. **(j)** *Evittia* sp. cf. *E. denticulata*. Stenlille-4, 1507.80 m; **(k)** *Neoveryhachium carminae.* Stenlille-4, 1502.15 m; **(l)** *Cymatiosphaera* sp. and large sphaeromorph. Stenlille-4, 1504.30 m.

that enhance the value of sedimentary provenance. And, given that reworking has not been generally observed in sedimentary sequences in the Triassic and Jurassic of NW Europe, the reworked material from the extinction interval in multiple locations across NW Europe represents a unique signal that can be linked to environmental changes that are constrained in time and space.

Reworking was not limited to the investigated cores. For example, sections in the Haida Gwaii Islands (Canada) contain a record of reworked Triassic conodonts that have been redeposited within the lowermost Jurassic (Greene et al., 2012). In the Mariental-1 core from

North Germany, reworked acritarchs are not as abundant as in Schandelah, but the presence of the Silurian acritarch *Multiplicisphaeridium* and Carboniferous spores was noted by Heunisch et al. (2010). These authors also described the reworking of typical Rhaetian pollen into Hettangian assemblages. Palynological analyses of the Kössen Formation and overlying Schattwald Beds in Austria by Bonis et al. (2009) show a remarkable increase in the diversity of trilete spores within the Schattwald Beds. Many of these taxa are however extremely rare, and most constitute single occurrences. It is not excluded that many of these taxa, including *Densosporites, Lycospora*, and *Cingulizonates* are in fact reworked Carboniferous taxa. The reworking of Carboniferous spores has been observed in several other previous studies on Hettangian to Sinemurian palynological assemblages, for example on Bornholm (Nielsen and Koppelhus, 1991), in the Paris Basin (Hagemann, 1967), in Poland (Muir, 1967) and in Northeast Scotland (Windle, 1979).

4.2. Clay minerals as indicators of soil erosion

Clay particles are aluminosilicate minerals, typically with a size of 2 μm or less, and they are the by-products of both physical weathering (e.g. mechanically weathered mica) and chemical weathering (so-called secondary minerals). The chemical pathway of clay mineral formation is a primary driver of soil formation (pedogenesis), and soils can store organic carbon, as clay particles have a high sorptive capacity (Hedges and Keil, 1995), thereby stabilizing soils and improving nutrient and water retention times (Ekwue, 1990). Clay formation occurs as poorly soluble ions, such as aluminum, form immobile hydrolyzates resistant to further weathering. This process is dictated largely by the large ionic radius and the high ionic charge of Al, and therefore Al has a tendency to form strong bonds with oxygen. On the other hand, chemical species with a small ionic radius and low ionic charge (Na, Ca, Mg and Li) are more readily weathered from the parent primary minerals, and are covered by a hydration shell once liberated, making them highly soluble. As such weathering intensity, which is described as a function of weathering rate and time of exposure, dictates the predominant mineralogy of the clay assemblage. Illites and montmorillonites are low intensity secondary products of weathering, while kaolinites are their intensely weathered counterparts (Nesbitt and Young, 1984).

A change in chemical weathering during the latest Triassic has been inferred from clay mineralogical studies. A sudden change in clay mineralogy in the upper Rhaetian is very obvious in sections of the northeastern Paris Basin. High kaolinite contents have been de described in the Argiles de Levallois in the Grouft drillcore (Luxembourg) by Lieder-Wolf (2012). Most of the other sections in this region (including Boust) show similar stratigraphic trends in clay mineralogy. Through the Rhaetian, the weathering became increasingly lateritic in nature, with an enrichment of iron-oxyhydroxides. The Argiles de Levallois therefore show a very characteristic reddish-brown colour, due to a high content of goethite and hematite. Additionally, the concentrations of iron and other siderophile trace elements are also relatively high (Kuhlmann, 2019*)*.

Increased amounts of kaolinite encountered in boundary beds across NW Europe have been taken as evidence for extremely humid conditions (van de Schootbrugge et al., 2009; Zajzon et al., 2012; Lintnerová et al., 2013). In Scania (Sweden), high amounts of kaolinite were identified in the uppermost Rhaetian Bjuv Member (Lindström and Erlström, 2006). Whereas the entire Late Triassic to Early Jurassic succession in Scania is characterized by deltaic and flood plain deposits that show evidence for intense chemical weathering of the Fennoscandian margin under humid climate conditions (Ahlberg et al., 2002), the Bjuv Member vertisols clearly stand-out compared to Lower Jurassic paleosoils (Ahlberg et al., 2003). The vertisol underclays constitute excellent kaolinitic clays for the ceramic industry (Ahlberg et al., 2003). Further south, sections in the Tatra Mountains in Slovakia show a strong increase in kaolinite content across the Rhaetian-Hettangian boundary (Michalik et al., 2010; Lintnerová et al., 2013) coinciding with an increase in fern spore abundance (Ruckwied and Götz, 2009). In Pakistan, kaolinite contents increases across the Rhaetian-Hettangian boundary together with sedimentological and petrographical evidence for a marked change in weathering and erosion (Iqbal et al., 2019). As discussed by Iqbal et al. (2019) the chemical index of alteration sharply increases also at the Rhaetian-Hettangian boundary. Towards the East, clay mineral analyses of a suite of cores from Poland show marked changes in clay mineraology starting with the precursor carbon isotope excursion in the Rhaetian (Pienkowski et al., 2014; Brański, 2014). In addition to an increase in kaolinite contents within the Triassic-Jurassic boundary beds, these authors also note an increase in osmium isotope values.

Although elevated proportions of kaolinite in Rhaetian sediments are usually related to enhanced chemical bedrock weathering, it is important to realize that the presence of clay in shallow-marine deposits could well be derived through physical erosion of soils and, more particularly, older clay-rich sediments (Thiry, 2000). In Europe, notably the extensive late Carboniferous clastic deposits are a plausible source of reworked kaolinite. Tethyan sections are illustrative for increased erosion rather than chemical weathering associated with the end-Triassic extinction, because in many Alpine and southern European sections carbonate deposition ceased prior to the Triassic-Jurassic boundary and was replaced by mudstone or clay deposition. The Schattwald Beds in the Northen Calcareous Alps (Austria) are a case-in-point, because this clay-rich unit overlaying the carbonate marl-limestone alternations of the Kössen Formation is the start of more generalized clay-rich sedimentation during the Early Jurassic (McRoberts et al., 1997). Although representing the southern margin of the Tethys, the sedimentological expression is remarkably similar in Italy, where the carbonate-rich Zu Formation of Rhaetian age is abruptly overlain by a distinct claystone at the base of the Malanotte Formation that marks the end-Triassic extinction event (Bachan et al., 2014; Galli et al., 2007). Although the cessation of carbonate deposition has been attributed to ocean acidification and a crisis in biocalcification in corals and other carbonate producing organisms (Hautmann et al., 2008; van de Schootbrugge et al., 2007), a widespread increase in erosion could also have led to smothering and eutrophication of shallow marine evironments, similar to what has been proposed for the end-Permian extinction (Algeo et al., 2011b; Algeo and Twitchett, 2010).

4.3. Provenance of the reworked material

Because of their taxonomic value and their general resistance to degradation, reworked palynomorphs are excellent tools to constrain sediment provenance. However, as pointed out by Streel and Bless (1980) and Batten (1991), all too often reworking is either ignored or reported only as accessory data, leaving its full potential unexplored. Nonetheless, several authors have successfully applied reworking to geological problems extending beyond glitches in biostratigraphy. For example, Truswell and Drewry (1984) used abundantly reworked Cretaceous palynomorphs to determine the provenance of sub-Recent sediments on the Antarctic shelf. Eshet et al. (1988) showed that regional sedimentary cycles throughout the Permian-Triassic subsurface of Israel corresponded to decreased (transgressive) and increased (regressive) levels of reworked palynomorphs. They noted specifically that reworking increased substantially as bedrock sourcing Palaeozoic palynomorphs became more exposed during regressive phases. In a recent study on the Carboniferous of Portugal it was found that more than 90% of the encountered palynomorphs were reworked from Cambrian to Devonian sediments that were part of the Variscan Orogeny. Understanding this regional reworking signal contributed signficantly to understanding basin geodynamical processes (Lopes et al., 2014). Reworked palynomorphs may even be used to showcase the former presence of sediments that are now long gone. Batten (1991) described reworking of Triassic and Jurassic palynomorphs in Tertiary sediments in Scotland, in an area that contains very few remnants of these

Mesozoic deposits.

We use the geological map of Fig. 1 to make predictions of probable source areas for the reworked assemblages encountered in the uppermost Rhaetian in our four studied cores. Palaeozoic acritarchs and chitinozoa present in the Stenlille palynological fraction were likely sourced directly from the Fennoscandia border zone towards the north. Previously, reworking of Carboniferous spores in the Lower Jurassic (Hettangian-Sinemurian) Rønne Formation on nearby Bornholm was reported by Nielsen and Koppelhus (1991) and attributed to erosion of uplifted blocks of basement and Palaeozoic cover along the southern limit of the Ringkøbing-Fyn high. However, it remains unclear whether these blocks were above water during much of the Early Jurassic. Alternatively, uplifted blocks in the Colonus Shale on the southern border of the Fennoscandian Shield could have been the source. The Palaeozoic cover in the area includes mostly Silurian, Ordovician, and Cambrian. Another potential source area could have been the area around Oslo, where the Oslo Confacies Belt comprises a thick series of Palaeozoic and Neoproterozoic sediments (Lassen and Thybo, 2012). Upper Silurian–lower Devonian strata are also present within the Sorgenfrei-Tornquist Zone in Scania, but Carboniferous–Permian sedimentary rocks are missing. Thus, the reworked Carboniferous spores and pollen found in strata in the Danish Basin may either have had a different source area, or alternatively the Carboniferous succession was completely removed at this event and later events during the Jurassic.

The rich and diverse assemblage of Ordovician and Silurian acritarchs encountered in the Triletes Beds in the Schandelah-1 core were most likely derived from outcrops in the Baltic Basin towards the East where much of the Palaeozoic strata must have been at the surface during the Triassic and Jurassic (Fig. 1). Paleogeographical reconstructions indicate the presence of a large deltaic system connecting the shallow marine areas in the Germanic Basin via Poland with the East European Platform in the hinterland (Barth et al., 2018a). In contrast, Franz and Wolfgramm (2008) proposed a Scandinavian source for the thick sandstone units within the Rhaetian Exter Formation that were transported via distributary channels reaching as far south as Lower Saxony and as far East as Mecklenburg-Vorpommern (Germany). Perhaps a more local source is also possible, for example with soil erosion taking place in the Rhenish Massif towards the south of Schandelah.

Two arguments for a local source can be made. The first is related to the presence of beds rich in clay clasts within the Triletes Beds in the Schandelah-1 core. Test analyses did not provide clear evidence that the clasts are the source of the reworked acritarchs, but the start of the clay clast beds does coincide with the onset in reworking (Fig. 10). The abundance of these clay clasts might suggest a local source. Furthermore, the ages of the reworked assemblages in the Schandelah-1 core appears to increase in age up section. Hence, there is clear evidence for an inverted stratigraphy with the younger Silurian material being eroded first and progressively older material (Ordovician and older) later. It appears unlikely that such a signal would be preserved if the material had been transported over hundreds of kilometers from Poland or the East European Platform. A local source from the Rhenish Massif towards the southwest or a Fennoscandian source is therefore likely.

The Neoproterozoic palynomorphs present in the Mingolsheim core were likely sourced from the Bohemian Massif towards the east of Mingolsheim (Fig. 1), even though the best preserved and most similar specimens in the literature have been described from the East European Platform. Neoproterozoic sediments with palynomorphs are known from the Czech Republic in the so-called Moravo-Silesian Unit or Brunovistulicum. Now buried beneath Carpathian Nappes, those Variscan units still reside at shallow depths (around 1000 m) and have remained relatively undeformed. Neoproterozoic sediments represent a former siliciclastic passive margin of Gondwana. Proterozoic sediments were folded and thrusted during the Variscan Orogeny and were covered by Silurian and Devonian siliciclastics and later by Carboniferous coal basins during foreland basin evolution (Kalvoda et al., 2008). Palynological work by several authors (e.g. Vavrdová, 2008) show rather poorly preserved Neoproterozoic palynomorphs in those units, which could be due to later thermal overprinting. It seems we have an interesting situtation, whereby the reworked palynomorphs that are now present in Mingolsheim are better preserved than their original source material.

The reworked palynomorphs present in the Boust core were almost certainly sourced from the London-Brabant Massif towards the north. In addition to Devonian limestones and siliciclastics, this ancient land mass is characterized by numerous outcrops of Carboniferous sedimentary rocks even today. During much of the Mesozoic it must have been shedding Palaeozoic material into shallow Mesozoic basins. The map in Fig. 1 can also be used to predict the predominant reworking signal observed, for example, in British Mesozoic basins, such as the Cardigan Bay and Cleveland basins. These basins were receiving mainly sediments derived from Carboniferous rocks, including the palynomorphs released from those sediments (Windle, 1979).

4.4. Mechanisms driving elevated soil erosion

Absolute quantitative data (pollen per gram of sediment) from the Mingolsheim core indicates that pollen accumulation decreased 1000-fold in the latest Rhaetian and did not recover until the middle Hettangian (Fig. 7e). This suggests that the drop in the abundance of tree pollen in the Triletes Beds across Germany, and in equivalent beds across NW Europe, reflects a true decrease in vegetation cover related to the end-Triassic crisis and, therefore, can not be ascribed to relative changes in organic matter fluxes. The widespread loss of arborescent vegetation, which can be traced from Sweden all the way south to Austria, can be regarded as the main cause for increased weathering and erosion during the latest Rhaetian. However, changes in vegetation, such as the shift to fern-dominated landscape during the Toarcian OAE (Slater et al., 2019), are not uncommon during the Mesozoic. While the TOAE has also been linked to elevated weathering and erosion (Dera et al., 2009; Them et al., 2017), there are no other reports of a similarly enhanced increase in the reworking of palynomorphs. Hence, it is likely that other additional mechanisms were at play during the end-Triassic extinction event.

Enhanced erosion during the latest Rhaetian was exacerbated by a number of reinforcing mechanisms that acted alongside deforestation. Large-scale tectonic events, such as large earthquakes, can trigger catastrophic landscape devastation as was observed in the aftermath of the 7.9 Mw Wenchuan earthquake that struck Sichuan province (China) in 2008. Seismic shaking led to catastrophic landslides, causing net topographic denudation (Ouimet, 2011). The latest Triassic in NW Europe contains unique evidence for repeated seismic activity not only in the Schandelah-1 core (Fig. 10; van de Schootbrugge et al., 2019), but also in Denmark, Sweden, Luxemburg and the United Kingdom (Lindström et al., 2015; Simms, 2003). Seismites, sedimentary layers that show typical signs of in situ shaking, such as slump folds, water-escape structures, and micro-faulting, occur over a wide area within the latest Triassic (Lindström et al., 2015). Whereas the pulses in reworking in the Schandelah-1 core are not directly coupled to the occurrences of the seismite beds (see also Fig. 10), the initiation of seismic activity does coincide with the start of influx of reworked material. The same observation can be made for the Boust core.

Enhanced erosion and run-off events can be triggered by loss of vegetation through burning (Sankey et al., 2017). Removal of vegetation due to burning not only leads to an increase in the impact of rain drops, but heating of soil may increase water repellency, stimulating run-off rather than uptake (Ferreira et al., 2008). There is good evidence for widespread fire activity during the Rhaetian from charcoal records from Germany (Uhl and Montenari, 2011), Greenland (Belcher et al., 2010), Sweden (Petersen and Lindstrom, 2012), and Poland (Marynowski and Simoneit, 2009). The increase in forest fire activity, despite overall lower oxygen concentrations in the atmosphere (Belcher

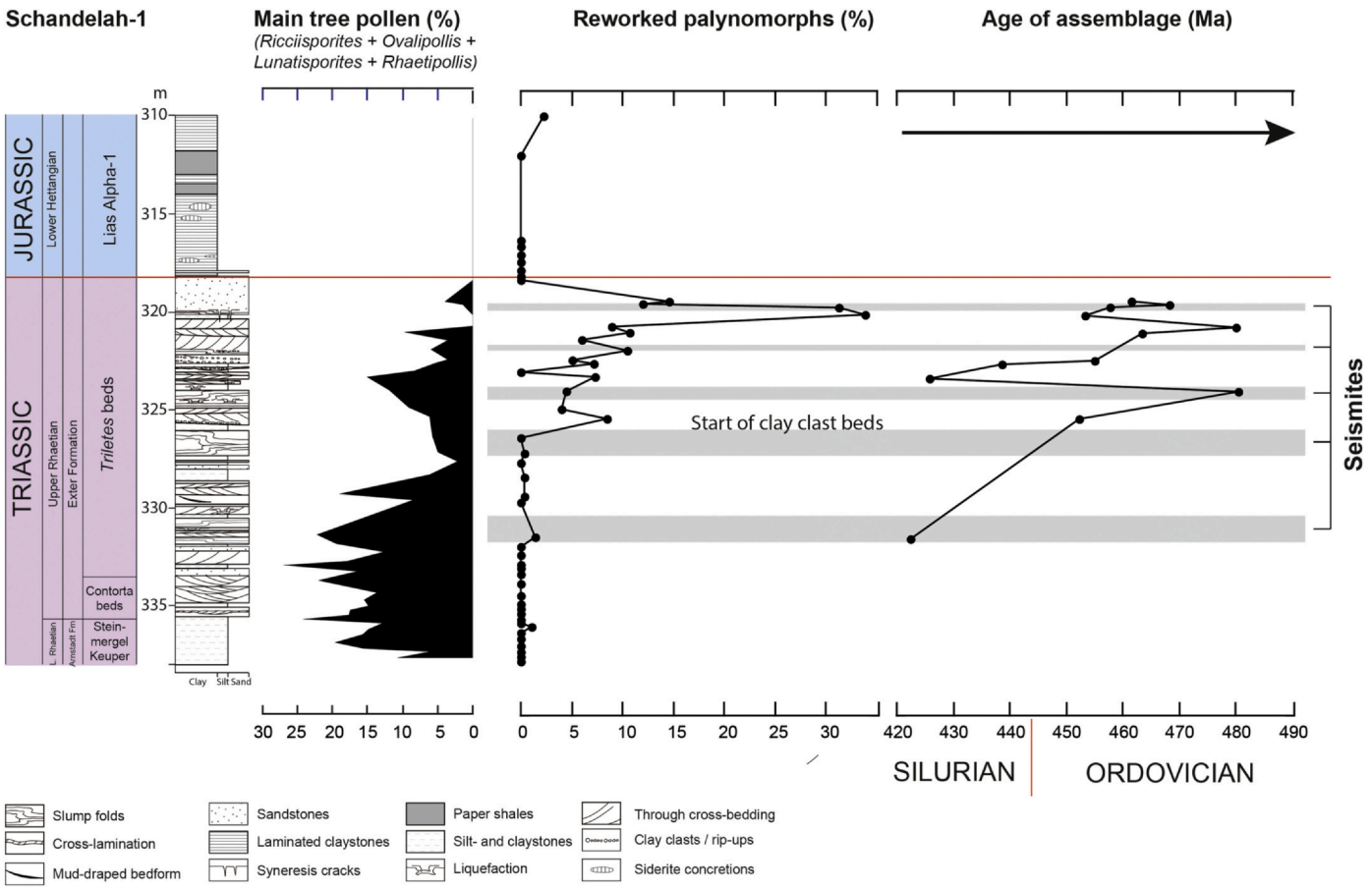

Fig. 10. Triassic-Jurassic boundary interval in the Schandelah-1 core. Reworking increases concommittantly with the onset of seismic activity and the reduction in tree cover. The age of the reworked assemblages shows an overall increase in age through the latest Rhaetian from mostly Silurian to predominantly Ordovician.

and McElwain, 2008), has been explained as a result of warming climates with a higher incidence of lightning strikes affecting plants that were increasingly prone to burning because of their finer leaves (Belcher et al., 2010; van de Schootbrugge, 2010). Importantly, all records of forest fires derive from the same geographical areas that also show elevated reworking, so it seems likely that landscape devastation due to burning also contributed to the observed phenomena.

Ultimately, weathering and erosion were also exacerbated by the release of large amounts of volatiles to the atmosphere, including CO_2 and SO_2, the latter of which would have had the potential via acid rain to increase weathering and erosion on short time scales. Basalts within the Central Atlantic Magmatic Province likely interacted with evaporites and coal in the subsurface, increasing their volatile load substantially (Callegaro et al., 2013, 2014; Heimdal et al., 2018). Sulfur aerosols would presumably not enter the stratosphere but instead would remain in the troposphere and rain out regionally. This could explain why the weathering signal is so unique especially in NW European basins, which would be downwind from the CAMP with the development of a permanent Inter-Tropical Convergence Zone (ITCZ) over Laurasia. In contrast to SO_2, carbon dioxide remains in the atmosphere much longer, and its effects therefore are very long lived. The duration of the Triletes Beds is estimated at perhaps 100 kyr or less, based on the latest timeline for CAMP eruptions and carbon isotope excursions presented by (Lindström et al., 2017). Whereas the long-term continuation of reworking during the Hettangian could be due to elevated atmospheric CO_2, it is unlikely that the massive increase in reworking in the latest Rhaetian would have been directly driven by carbon injection.

4.5. Biodegradation of palynomorphs and soil loss and resilience

In Quaternary studies the corrosion (biological and chemical alteration) of sporomorphs has been used to indicate erosion of lake catchments. In those studies, higher numbers of reworked palynomorphs correlate to a larger number of corroded specimens, indicating a positive correlation between erosion and corrosion (Wilmshurst and McGlone, 2005). Mander et al. (2012b) have used corrosion of palynomorphs in Triassic-Jurassic deposits in Greenland to examine the role of taphonomy in apparent mismatches between macro- and microfloral records. Although these authors did not distinguish between biological and chemical degradation, their plant bed 5, which represents the extinction interval in Greenland, did indeed show a higher incidence of corrosion. Microbial activity in mesophiles is known to be temperature dependent (Biederbeck and Campbell, 1973), hence metabolic rates of fungi and bacteria, likely increased during periods of global warming such as that seen across the Triassic-Jurassic boundary. We therefore fully expected to observe an increase in biodegradation of spores within the Triletes Beds.

The three intervals within the Schandelah core characterized by high numbers of reworked palynomorphs, however, clearly show much lower numbers of biodegraded spores (Fig. 7). Although seemingly counter-intuitive, in our recorded decrease in biodegradation is compatible with records of increased reworking in the same intervals. As our records of intense reworking of Palaeozoic and older bedrock material clearly show, it is entirely plausible that soils were already mostly removed during deposition of the Triletes Beds as a result of deforestation and erosion. Instead of being retained in soils, eroded palynomorphs would have bypassed soils and have been washed out directly to shallow marine settings where they were subsequently

preserved without retaining evidence of microbial degradation.

Additional factors that could stymie biodegradation include high runoff from intensified precipitation, flushing organic matter more rapidly into estuaries and coastal seas. High runoff has been inferred by several authors using palynological data. Bonis and Kürschner (2012) interpreted elevated counts of fern spores within the Schattwald beds, the Austrian equivalent of the German Triletes Beds, mainly as an indication of wet conditions. In their scenario, climate change induced by CAMP eruptions led to stronger monsoonal rainfall and increased runoff. A similar conclusion was reached by Ruckwied and Götz (2009) based on an increase in fern spores within the transition from the uppermost Rhaetian Fatra Formation to the lower Hettangian Kopieniec Formation in Slovakia. In addition, based on changes in the chemical alteration index of their palynomorphs, Iqbal et al. (2019) proposed a significant increase in humidity across the Rhaetian-Hettangian boundary.

The increase in the amount of biodegraded spores in the lower Hettangian of the Schandelah core is interpreted to indicate terrestrial ecosystem recovery (Fig. 7). High soil microbial diversity and abundance reflects a healthy ecosystem (Coleman et al., 1992). Following the initial recovery of biodegradation, reaching plateau values within the Liasicus Zone, two sharp declines in the abundance of biodegraded spores are evident associated with the two enigmatic red beds in the upper Hettangian (Fig. 7). In accordance with high levels of biodegradation representing a healthy ecosystem, these drops in biodegradation are here interpreted as renewed environmental perturbations. This would have resulted in decreased microbial activity and diversity, hence a decrease in sporomorph biodegradation.

Much lower rates of reworking during the Hettangian may have been driven by recovery of arborescent vegetation, as is clear from the recovery of tree pollen abundance in our long-term record from the Schandelah-1 core (Fig. 7). This may have slowed down the most intense erosion. In this light it is notable that photic zone euxinia (PZE) also decreased or ceased altogether with a return of biodegraded spores within the basal Hettangian. General amelioration of conditions both on land and in the oceans may also be inferred from the first occurrence of ammonites (*Neophyllites* sp.) around 312 mbs (van de Schootbrugge et al., 2019), which is the horizon where biodegradation of spores reaches a stable level.

Constraining sediment fluxes across the Rhaetian-Hettangian boundary is crucial for understanding the underlying causes for intense marine PZE that spread during the earliest Jurassic in the Tethys and Panthalassa Oceans (Richoz et al., 2012; Jaraula et al., 2013; Kasprak et al., 2015). Although likely caused by a myriad of reinforcing feedback mechanisms, including global warming and stratification, anoxic events are generally linked to eutrophication of surface waters through enhanced land-derived input of phosphorus and other biolimiting nutrients (Jenkyns, 2003). Intense anoxia in coastal seas during the early Hettangian coincided with first order sea level rise causing long-term flooding and deepening of basins across NW Europe (Barth et al., 2018b). This major Jurassic transgression initially impinged on land masses that contained large amounts of freshly weathered regolith, creating ideal conditions for surplus nutrients in shallow coastal areas. Such a model has been suggested for other phases of Jurassic near-shore anoxia related to transgression onto coastal margins (Leonowicz, 2016).

5. Conclusions

There is strong evidence for intense soil erosion on continental landmasses surrounding basins in NW Europe, the timing of which overlaps with the emplacement of the CAMP. Latest Rhaetian sediments deposited in different basins across NW Europe record a dramatic increase in reworking of Palaeozoic and Neoproterozoic palynomorphs derived from eroded soil and regolith. Depending on the location, the composition and age of the reworked material is different. Danish and North German Basins retain mostly Ordovician and Silurian acritarchs and prasinophytes, along with lesser numbers of Devonian, Carboniferous and Middle–early Late Triassic palynomorphs that were washed in from Fennoscandia and the Baltic Platform. In the South German Basin, Neoproterozoic material was likely derived from the Bohemian Massif. The Paris Basin retained mostly Carboniferous reworked palynomorphs, which were derived from the London-Brabant Massif. Increased erosion corresponded with the disappearance of dominant Triassic pollen taxa and a proliferation in fern spores. Deforestation, therefore, was the driving mechanism behind this major increase in erosion. Denudation of the Triassic landscape is evident from an inverted stratigraphy, whereby the age of the reworked material increases upsection. This indication of bedrock erosion further implies a general loss of soil cover. In addition to deforestation as a direct result of volcanism, earthquakes and forest fires all contributed to soil loss across the Triassic-Jurassic boundary.

Declaration of Competing Interest

None.

Acknowledgments

BvdS acknowledges financial support from the Goethe University Frankfurt (Frankfurt am Main, Germany) allowing to drill the Schandelah core. BvdS and PKS acknowledge financial support from the German Science Foundation (DFG) grant# SCH1216/5-1. SL acknowledges support from GEUS. Alexander Houben (TNO) is thanked for help with the identification of Carboniferous spores. Natasja Welters is thanked for her help with processing the palynological samples at Utrecht University.

References

Ahlberg, A., Arndorff, L., Guy-Ohlson, D., 2002. Onshore climate changes during the late Triassic marine inundation of the central European Basin. Terra Nova 14, 241–248.
Ahlberg, A., Olsson, I., Šimkevičius, P., 2003. Triassic–Jurassic weathering and clay mineral dispersal in basement areas and sedimentary basins of southern Sweden. Sediment. Geol. 161 (1–2), 15–29.
Algeo, T.J., Twitchett, R.J., 2010. Anomalous early Triassic sediment fluxes due to elevated weathering rates and their biological consequences. Geology 38, 1023–1026.
Algeo, T.J., Chen, Z.Q., Fraiser, M.L., Twitchett, R.J., 2011a. Terrestrial–marine teleconnections in the collapse and rebuilding of early Triassic marine ecosystems. Palaeogeogr. Palaeoclimatol. Palaeoecol. 308 (1–2), 1–11.
Algeo, T.J., Kuwahara, K., Sano, H., Bates, S., Lyons, T., Elswick, E., Hinnov, L., Ellwood, B., Moser, J., Maynard, J.B., 2011b. Spatial variation in sediment fluxes, redox conditions, and productivity in the Permian–Triassic Panthalassic Ocean. Palaeogeogr. Palaeoclimatol. Palaeoecol. 308 (1–2), 65–83.
Bachan, A., van de Schootbrugge, B., Payne, J.L., 2014. The end-Triassic negative $\delta^{13}C$ excursion: a lithologic test. Palaeogeogr. Palaeoclimatol. Palaeoecol. 412, 177–186.
Bacon, K.L., Belcher, C.M., Hesselbo, S.P., McElwain, J.C., 2011. The Triassic-Jurassic boundary carbon isotope excursions expressed in taxonomically identified leaf cuticles. Palaios 26, 461–469.
Barth, G., Franz, M., Heunisch, C., Ernst, W., Zimmermann, J., Wolfgramm, M., 2018a. Marine and terrestrial sedimentation across the T–J transition in the north German Basin. Palaeogeogr. Palaeoclimatol. Palaeoecol. 489, 74–94.
Barth, G., Pieńkowski, G., Zimmermann, J., Franz, M., Kuhlmann, G., 2018b. Palaeogeographical evolution of the Lower Jurassic: High-Resolution Biostratigraphy and Sequence Stratigraphy in the Central European Basin. Geological Society, London Special Publications: SP469.8.
Batten, D.J., 1991. Reworking of plant microfossils and sedimentary provenance. In: Todd, S.P., Haughton, P.D.W. (Eds.), A.C. Morton. Geological Society Special Publication, Developments in Sedimentary Provenance Studies, pp. 79–90.
Belcher, C.M., McElwain, J.C., 2008. Limits for combustion in low O2 redefine paleoatmospheric predictions for the Mesozoic. Science 321 (5893), 1197–1200.
Belcher, C.M., Mander, L., Rein, G., Jervis, F.X., Haworth, M., Hesselbo, S.P., Glasspool, I.J., McElwain, J.C., 2010. Increased fire activity at the Triassic/Jurassic boundary in Greenland due to climate-driven floral change. Nat. Geosci. 3 (6), 426–429.
Biederbeck, V.O., Campbell, C.A., 1973. Soil microbial activity as influenced by temperature trends and fluctuations. Can. J. Soil Sci. 53, 363–376.
Bonis, N.R., Kürschner, W.M., 2012. Vegetation history, diversity patterns, and climate change across the Triassic/Jurassic boundary. Paleobiology 38 (2), 240–264.
Bonis, N.R., Kürschner, W.M., Krystyn, L., 2009. A detailed palynological study of the Triassic-Jurassic transition in key sections of the Eiberg Basin (Northern Calcareous Alps, Austria). Rev. Palaeobot. Palynol. 156, 376–400.
Bonis, N.R., Ruhl, M., Kürschner, W.M., 2010. Milankovitch-scale palynological turnover across the Triassic-Jurassic transition at St Audrie's Bay, SW UK. J. Geol. Soc. Lond. 167, 877–888.

Brański, P., 2014. Climatic disaster at the Triassic-Jurassic boundary - a clay minerals and major elements record from the Polish Basin. Geol. Q. 58 (2).
Callegaro, S., Marzoli, A., Bertrand, H., Chiaradia, M., Reisberg, L., Meyzen, C., Bellieni, G., Weems, R.E., Merle, R., 2013. Upper and lower crust recycling in the source of CAMP basaltic dykes from southeastern North America. Earth Planet. Sci. Lett. 376, 186–199.
Callegaro, S., Baker, D.R., De Min, A., Marzoli, A., Geraki, K., Betrand, H., Viti, C., Nestola, F., 2014. Microanalyses link sulfur from large igneous provinces and Mesozoic mass-extinctions. Geology. 42, 895–898.
Cirilli, S., Marzoli, A., Tanner, L., Bertrand, H., Buratti, N., Jourdan, F., Bellieni, G., Kontak, D., Renne, P.R., 2009. Latest Triassic onset of the Central Atlantic Magmatic Province (CAMP) volcanism in the Fundy Basin (Nova Scotia): New stratigraphic constraints. Earth Planet. Sci. Lett. 286, 514–525.
Clayton, G., Coquel, R., Doubinger, J., Gueinn, K.J., Loboziak, S., Owens, B., Streel, M., 1977. Carboniferous miospores of Western Europe: illustration and zonation. Mededelingen Rijksgeologische Dienst 29, 1–71.
Coleman, D.C., Odum, E.P., Crossley, D.A., 1992. Soil biology, soil ecology, and global change. Biol. Fertil. Soils 14, 104–111.
Cox, R., Zentner, D.B., Rakotondrazafy, A.F.M., Rasoazanamparany, C.F., 2010. Shakedown in Madagascar: Occurrence of lavakas (erosional gullies) associated with seismic activity. Geology 38 (2), 179–182.
Cushing, E.J., 1967. Evidence for differential pollen preservation in late Quaternary sediments in Minnesota. Rev. Palaebot. Palynol. 4, 87–101.
Czeczuga, B., Muszynska, E., 2001. Zoosporic fungi growing on gymnosperm pollen in water of varied trophic state. Pol. J. Environ. Stud. 10, 89–94.
Dera, G., Pellenard, P., Neige, P., Deconinck, J.-F., Puceat, E., Dommergues, J.-L., 2009. Distribution of clay minerals in early Jurassic Peritethyan seas: Palaeoclimatic significance inferred from multiproxy comparisons. Palaeogeogr. Palaeoclimatol. Palaeoecol. 271, 39–51.
Drever, J.I., 1994. The effect of land plants on weathering rates of silicate minerals. Geochim. Cosmochim. Acta 58, 2325–2332.
Ekwue, E.I., 1990. Organic-matter effects on soil strength properties. Soil Tillage Res. 16, 289–297.
Eshet, Y., Druckman, Y., Cousminer, H.L., Habib, D., Drugg, W.S., 1988. Reworked palynomorphs and their use in the determination of sedimentary cycles. Geology 16, 662–665.
Ferreira, A.J.D., Coelho, C.O.A., Ritsema, C.J., Boulet, A.K., Keizer, J.J., 2008. Soil and water degradation processes in burned areas: Lessons learned from a nested approach. Catena 74 (3), 273–285.
Fowell, S.J., Cornet, B., Olsen, P.E., 1994. Geologically rapid late Triassic extinctions: Palynological evidence from the Newark Supergroup. In: Klein, G.D. (Ed.), Pangea: Paleoclimate, Tectonics, and Sedimentation during Accretion, Zenith and Break-Up of a Supercontinent. Geological Society of America, Boulder, CO.
Franz, M., Wolfgramm, M., 2008. Sedimentology, petrology and facies of geothermal reservoirs of the north German Basin - the example of the Exter Formation (Upper Keuper, Rhaetian) of NE Germany. Z. Geol. Wiss. 36, 223–247.
Freckman, D.W., Blackburn, T.H., Brussaard, L., Hutchings, P., Palmer, M.A., Snelgrove, P.V.R., 1997. Linking biodiversity and ecosystem functioning of soils and sediments. Ambio 26, 556–562.
French, K.L., Tosca, N.J., Cao, C., Summons, R.E., 2012. Diagenetic and detrital origin of moretane anomalies through the Permian–Triassic boundary. Geochim. Cosmochim. Acta 84, 104–125.
Galli, M.T., Jadoul, F., Bernasconi, S.M., Ciriili, S., Weissert, H., 2007. Stratigraphy and palaeoenvironmental analysis of the Triassic-Jurassic transition in the western Southern Alps (Northern Italy). Palaeogeogr. Palaeoclimatol. Palaeoecol. 244, 52–70.
Goldstein, S., 1960. Degradation of pollen by phycomycetes. Ecology 41, 543–545.
Götz, A.E., Ruckwied, K., Palfy, J., Haas, J., 2009. Palynological evidence for synchronous changes within the terrestrial and marine realm at the Triassic-Jurassic boundary (Csövàr section, Hungary). Rev. Palaeobot. Palynol. 156, 401–409.
Greene, S.E., Bottjer, D.J., Corsetti, F.A., Berelson, W.M., Zonneveld, J.-P., 2012. A subseafloor carbonate factory across the Triassic-Jurassic transition. Geology 40, 1043–1046.
Grice, K., Cao, C., Love, G.D., Bottcher, M.E., Twitchett, R.J., Grosjean, E., Summons, R.E., Turgeon, S.C., Dunning, W., Jin, Y., 2005. Photic zone euxinia during the Permian-triassic superanoxic event. Science 307 (5710), 706–709.
Hagemann, H.W., 1967. Umgelagerst Karbonsporen aus den Rhaet-Lias-Schichten SE-Luxemburgs. Publ. Service Geol. Luxembourg 17, 207–221.
Hautmann, M., Benton, M.J., Tomasovych, A., 2008. Catastrophic Ocean acidification at the Triassic-Jurassic boundary. N. Jb. Geol. Paläont. (Abh.) 249, 119–127.
Havinga, A.J., 1967. Palynology and pollen preservation. Rev. Palaeobot. Palynol. 2, 81–98.
Hedges, J.I., Keil, R.G., 1995. Sedimentary organic matter preservation: an assessment and speculative synthesis. Mar. Chem. 49, 81–115.
Heimdal, T.H., Svensen, H.H., Ramezani, J., Iyer, K., Pereira, E., Rodrigues, R., Jones, M.T., Callegaro, S., 2018. Large-scale sill emplacement in Brazil as a trigger for the end-Triassic crisis. Sci. Rep. 8 (1), 141.
Hettich, M., 1974. Ein vollständiges Rhät/Lias-Profil aus der Langenbrückener Senke, Baden-Württemberg (Kernbohrung Mingolsheim 1968). Geol. Jahrb. A16, 75–105.
Heunisch, C., Luppold, F.W., Reinhardt, L., Röhling, H.-G., 2010. Palynofazies, Bio-, und Lithostratigraphie im Grenzbereich Trias/Jura in der Bohrung Mariental I (Lappwaldmulde, Ostniedersachsen). Z. Dtsch. Geol. Ges. 161, 51–98.
Iqbal, S., Wagreich, M., Irfan, U., Kuerschner, W.M., Gier, S., Bibi, M., 2019. Hot-house climate during the Triassic/Jurassic transition: the evidence of climate change from the southern hemisphere (Salt Range, Pakistan). Glob. Planet. Chang. 172, 15–32.
Isozaki, Y., 1997. Permian-Triassic boundary super anoxia and stratified superocean: records from lost deep sea. Science 276, 235–238.
Isozaki, Y., Shimizu, N., Yao, J., Ji, Z., Matsuda, T., 2007. End-Permian extinction and volcanism-induced environmental stress: the Permian–Triassic boundary interval of lower-slope facies at Chaotian, South China. Palaeogeogr. Palaeoclimatol. Palaeoecol. 252 (1–2), 218–238.
Jaraula, C.M.B., Grice, K., Twitchett, R.J., Bottcher, M.E., LeMetayer, P., Dastidar, A.G., Opazo, L.F., 2013. Elevated pCO_2 leading to late Triassic extinction, persistent photic zone euxinia, and rising sea levels. Geology 41 (9), 955–958.
Jenkyns, H.C., 2003. Evidence for rapid climate change in the Mesozoic-Palaeogene greenhouse world. Philos. Trans. R. Soc. Lond. A 361, 1885–1916.
Jiao, D., Perry, R.S., Engel, M.H., Sephton, M.A., 2008. Biomarker Indicators of Bacterial Activity and Organic Fluxes during End Triassic Mass Extinction Event. Optical engineering + applications, San Diego.
Jost, A.B., Bachan, A., van de Schootbrugge, B., Lau, K.V., Weaver, K.L., Maher, K., Payne, J.L., 2017. Uranium isotope evidence for an expansion of marine anoxia during the end-Triassic extinction. Geochem. Geophys. Geosyst. https://doi.org/10.1002/2017GC006941.
Kaiho, K., Koga, S., 2013. Impacts of a massive release of methane and hydrogen sulfide on oxygen and ozone during the late Permian mass extinction. Glob. Planet. Chang. 107, 91–101.
Kaiho, K., Saito, R., Ito, K., Miyaji, T., Biswas, R., Li, T., Sano, H., Shi, Z., Takahashi, S., Tong, J., 2016. Effects of soil erosion and anoxic-euxinic ocean in the Permian–Triassic marine crisis. Heliyon 2, e00137.
Kalvoda, J., Babek, O., Fatka, O., Leichmann, J., Melichar, R., Nehyba, S., Spacek, P., 2008. Brunovistulian terrane (Bohemian Massif, Central Europe) from late Proterozoic to late Paleozoic: a review. Int. J. Earth Sci. 97, 497–518.
Kasprak, A.H., Sepulveda, J., Price-Waldman, R., Williford, K.H., Schoepfer, S.D., Haggart, J.W., Ward, P.D., Summons, R.E., Whiteside, J.H., 2015. Episodic photic zone euxinia in the northeastern Panthalassic Ocean during the end-Triassic extinction. Geology 43 (4), 307–310.
Kuhlmann, N., 2019. Untersuchungen der paläogeographischen, paläoklimatischen, umweltgeologischen und paläoökologischen Verhältnisse in der Oberen Trias und im Unteren Jura im NE Pariser Becken (Luxemburg/Südeifel/Lothringen), unter besonderer Berücksichtigung des Endtriassischen Massenaussterbeereignisses. pp. 278.
Lassen, A., Thybo, H., 2012. Neoproterozoic and Palaeozoic evolution of SW Scandinavia based on integrated seismic interpretation. Precambrian Res. 204-205, 75–104.
Leonowicz, P., 2016. Nearshore transgressive black shale from the Middle Jurassic shallow-marine succession from southern Poland. Facies 62 (2).
Li, G., Pang, K., Chen, L., Zhou, G., Han, C., Yang, L., Wang, W., Yang, F., Yin, L., 2019. Organic-walled microfossils from the Tonian Tongjiazhuang Formation of the Tumen Group in western Shandong, North China Craton and their biostratigraphic significance. Gondwana Res. 76, 260–289.
Lieder-Wolf, H., 2012. Untersuchungen zur Tonmineralogie im Trias/Jura Grenzbereich in Luxemburg, Bonn University, unpubl. Master thesis. pp. 56.
Lindström, S., 2016. Palynofloral patterns of terrestrial ecosystem change during the end-Triassic event – a review. Geol. Mag. 153, 223–251.
Lindström, S., Erlström, M., 2006. The late Rhaetian transgression in southern Sweden: Regional (and global) recognition and relation to the Triassic–Jurassic boundary. Palaeogeogr. Palaeoclimatol. Palaeoecol. 241 (3–4), 339–372.
Lindström, S., van de Schootbrugge, B., Dybkjaer, K., Pedersen, G.K., Fiebig, J., Nielsen, L.H., Richoz, S., 2012. No causal link between terrestrial ecosystem change and methane release during the end-Triassic mass-extinction. Geology 40, 531–534.
Lindström, S., Pedersen, G.K., van de Schootbrugge, B., Hansen, K.H., Kuhlmann, N., Thein, J., Johansson, L., Petersen, H.I., Alwmark, C., Dybkjær, K., Weibel, R., Erlström, M., Nielsen, L.H., Oschmann, W., Tegner, C., 2015. Intense and widespread seismicity during the end-Triassic mass extinction due to emplacement of a large igneous province. Geology 43 (5), 387–390.
Lindström, S., van de Schootbrugge, B., Hansen, K.H., Pedersen, G.K., Alsen, P., Thibault, N., Dybkjær, K., Bjerrum, C.J., Nielsen, L.H., 2017. A new correlation of Triassic–Jurassic boundary successions in NW Europe, Nevada and Peru, and the Central Atlantic Magmatic Province: a time-line for the end-Triassic mass extinction. Palaeogeogr. Palaeoclimatol. Palaeoecol. 478, 80–102.
Lintnerová, O., Michalík, J., Uhlík, P., Soták, J., 2013. Latest Triassic climate humidification and kaolinite formation (Western Carpathians, Tatric Unit of the Tatra Mts). Geol. Q. 57 (4).
Looy, C.V., Twitchett, R.J., Dilcher, D.L., van Konijnenburg-Van Cittert, J.H.A., Visscher, H., 2001. Life in the end-Permian dead zone. Proc. Natl. Acad. Sci. 98, 7879–7883.
Lopes, G., Pereira, Z., Fernandes, P., Wicander, R., Matos, J.X., Rosa, D., Oliveira, J.T., 2014. The significance of reworked palynomorphs (middle Cambrian to Tournaisian) in the Visean Toca da Moura complex (South Portugal). Implications for the geodynamic evolution of Ossa Morena Zone. Rev. Palaeobot. Palynol. 200, 1–23.
Loron, C.C., Rainbird, R.H., Turner, E.C., Greenman, J.W., Javaux, E.J., 2019. Organic-walled microfossils from the late Mesoproterozoic to early Neoproterozoic lower Shaler Supergroup (Arctic Canada): Diversity and biostratigraphic significance. Precambrian Res. 321, 349–374.
Lund, J.J., 1977. Rhaetic to lower Liassic palynology of the on-shore South-Eastern North Sea Basin. Dan. Geol. Unders. 109, 1–112.
Luo, G., Richoz, S., van de Schootbrugge, B., Algeo, T.J., Xie, S., Ono, S., Summons, R.E., 2018. Multiple sulfur-isotopic evidence for a shallowly stratified ocean following the Triassic-Jurassic boundary mass extinction. Geochim. Cosmochim. Acta 231, 73–87.
Mander, L., Collinson, M.E., Chaloner, W.G., Brain, A.P.R., Long, D.G., 2012a. The Ultrastructure and Botanical Affinity of the Problematic Mid-Mesozoic Palynomorph *Ricciisporites tuberculatus* Lundblad. Int. J. Plant Sci. 173 (4), 429–440.
Mander, L., Wesseln, C.J., McElwain, J.C., Punyasena, S.W., 2012b. Tracking taphonomic regimes using chemical and mechanical damage of pollen and spores: an example from the Triassic-Jurassic mass extinction. PLoS One 7 (11), e49153.
Marynowski, L., Simoneit, B.R.T., 2009. Widespread Upper Triassic to lower Jurassic wildfire records from Poland: Evidece from charcoal and pyrolytic polycyclic aromatic hydrocarbons. Palaios 24, 785–798.
McElwain, J.C., Beerling, D.J., Woodward, F.I., 1999. Fossil plants and global warming at the Triassic-Jurassic boundary. Science 285, 1386–1390.
McRoberts, C.A., Furrer, H., Jones, D.S., 1997. Palaeoenvironmental interpretation of a Triassic-Jurassic boundary section from Western Austria based on palaeoecological and geochemical data. Palaeogeogr. Palaeoclimatol. Palaeoecol. 136 (1–4), 79–95.
Mehlqvist, K., Steemans, P., Vajda, V., 2015. First evidence of Devonian strata in

Sweden—a palynological investigation of Övedskloster drillcores 1 and 2, Skåne, Sweden. Rev. Paleobot. Palynol. 122, 144–159.
Michalik, J., Biron, A., Lintnerova, O., Gotz, A.E., Ruckwied, K., 2010. Climate change at the Triassic/Jurassic boundary in the northwestern Tethyan realm, inferred from sections in the Tatra Mountains (Slovakia). Acta Geol. Pol. 60, 535–548.
Muir, M.D., 1967. Reworking in Jurassic and cretaceous spore assemblages. Rev. Palaeobot. Palynol. 5, 145–154.
Nesbitt, H.W., Young, G.M., 1984. Prediction of some Weathering Trends of Plutonic and Volcanic-Rocks based on Thermodynamic and Kinetic Considerations. Geochim. Cosmochim. Acta 48, 1523–1534.
Newell, A.J., Sennikov, A.G., Benton, M.J., Molostovskaya, I.I., Golubev, V.K., Minikh, A.V., Minikh, M.G., 2010. Disruption of playa lacustrine depositional systems at the Permo–Triassic boundary: evidence from Vyazniki and Gorokhovets on the Russian Platform. J. Geol. Soc. 167, 695–716.
Nielsen, L.H., 2003. Late Triassic – Jurassic development of the Danish Basin and the Fennoscandian Border Zone, southern Scandinavia. Geol. Survey Denmark Greenland Bull. 1, 459–526.
Nielsen, L.H., Koppelhus, E.B., 1991. Reworked Carboniferous palynomorphs from the lower Jurassic of Bornholm and their palaeogeographic significance. Bull. Geol. Soc. Denmark 38, 253–266.
Olsson-Borell, I., Ahlberg, A., 2003. Contact metamorphism of Palaeozoic shale in southern Sweden: Influences on clay mineralogy and implications for railway construction material properties. GFF 125, 63–68.
Orgiazzi, A., Bardgett, R.D., Barrios, E., Behan-Pelletier, V., Briones, M.J.I., Chotte, J.-L., De Deyn, G.B., Eggleton, P., Fierer, N., Fraser, T., Hedlund, K., Jeffery, S., Johnson, N.C., Jones, A., Kandeler, E., Kaneko, N., Lavelle, P., Lemanceau, P., Miko, L., Montanarella, L., Moreira, F.M.S., Ramirez, K.S., Scheu, S., Singh, B.K., Six, J., van der Putten, W.H., Wall, D.H., 2016. Global Soil Biodiversity Atlas. European Commission, Luxembourg, pp. 176.
Ouimet, W.B., 2011. Tectonic geomorphology: the hills came tumbling down. Nat. Geosci. 4 (7), 424–425.
Petersen, H.I., Lindstrom, S., 2012. Synchronous wildfire activity rise and mire deforestation at the triassic-jurassic boundary. PLoS One 7 (10), e47236.
Pienkowski, G., Niedzwiedzki, G., Branski, P., 2014. Climatic reversals related to the Central Atlantic Magmatic Province caused the end-Triassic biotic crisis - evidence from continental strata in Poland. In: Keller, G., Kerr, A. (Eds.), Volcanism, Impacts, and Mass-Extinctions: Causes and Effects, (Geological Society of America).
Quan, T., van de Schootbrugge, B., Field, P., Rosenthal, Y., Falkowski, P.G., 2008. Nitrogen isotope and trace metal analyses from the Mingolsheim core (Germany): evidence for redox variations across the Triassic-Jurassic boundary. Glob. Biogeochem. Cycles 22, GB2014.
Retallack, G.J., Metzger, C.A., Greaver, T., Jahren, A.H., Smith, R.M.H., Sheldon, N.D., 2006. Middle-late Permian mass extinction on land. Geol. Soc. Am. Bull. 118 (11 – 12), 1398–1411.
Richoz, S., van de Schootbrugge, B., Pross, J., Püttmann, W., Quan, T.M., Lindström, S., Heunisch, C., Fiebig, J., Maquil, R., Hauzenberger, C., Schouten, S., Wignall, P.B., 2012. Hydrogen sulphide poisoning of shallow seas due to end-Triassic global warming. Nat. Geosci. 5, 662–667.
Ruckwied, K., Götz, A.E., 2009. Climate change at the Triassic/Jurassic boundary: palynological evidence from the Furkaska section (Tatra Mountains, Slovakia). Geol. Carpath. 60, 139–149.
Ruhl, M., Kürschner, W.M., 2011. Multiple phases of carbon cycle disturbance from large igneous province formation at the Triassic-Jurassic transition. Geology 39 (5), 431–434.
Ruhl, M., Bonis, N.R., Reichart, G.-J., Sinninghe Damste, J.S., Kürschner, W., 2011. Atmospheric carbon injection linked to end-Triassic mass-extinction. Science 333, 430–434.
Sankey, J.B., Kreitler, J., Hawbaker, T.J., McVay, J.L., Miller, M.E., Mueller, E.R., Vaillant, N.M., Lowe, S.E., Sankey, T.T., 2017. Climate, wildfire, and erosion ensemble foretells more sediment in western USA watersheds. Geophys. Res. Lett. 44 (17), 8884–8892.
Sawada, K., Kaiho, K., Okano, K., 2012. Kerogen morphology and geochemistry at the Permian–Triassic transition in the Meishan section, South China: Implication for paleoenvironmental variation. J. Asian Earth Sci. 54-55, 78–90.
Scharlemann, J.P.W., Tanner, E.V.J., Hiederer, R., Kapos, V., 2014. Global soil carbon: understanding and managing the largest terrestrial carbon pool. Carbon Manag. 5 (1), 81–91.
Sephton, M.A., Looy, C.V., Brinkhuis, H., Wignall, P.B., de Leeuw, J.W., Visscher, H., 2005a. Catastrophic soil erosion during the end-Permian biotic crisis. Geology 33 (12), 941–944.
Sephton, M.A., Looy, C.V., Visscher, H., Brinkhuis, H., De Leeuw, J.W., 2005b. In: Koeberl, H.C. (Ed.), The combined petrographic and geochemical analysis of end-Permian kerogens. Impact Tectonics, Springer, New York, pp. 467–478.
Shen, W., Lin, Y., Xu, L., Li, J., Wu, Y., Sun, Y., 2007. Pyrite framboids in the Permian–Triassic boundary section at Meishan, China: evidence for dysoxic deposition. Palaeogeogr. Palaeoclimatol. Palaeoecol. 253 (3–4), 323–331.
Simms, M.J., 2003. Uniquely extensive seismite from the latest Triassic of the United Kingdom: evidence for bolide impact? Geology 31, 557–560.
Skvarla, J.J., Anderegg, D.E., 1972. Infestation of cedar pollen by *Rhizophidium* (chytridiomycetes). Grana 12 (1), 47–51.
Slater, S.M., Twitchett, R.J., Danise, S., Vajda, V., 2019. Substantial vegetation response to early Jurassic global warming with impacts on oceanic anoxia. Nat. Geosci. 12 (6), 462–467.
Smith, R.M.H., 1995. Changing fluvial environments across the Permian-Triassic boundary in the Karoo Basin, South Africa and possible causes of tetrapod extinctions. Palaeogeogr. Palaeoclimatol. Palaeoecol. 117, 81–104.
Steinthorsdottir, M., Jeram, A.J., McElwain, J.C., 2011. Extremely elevated CO_2 concentrations at the Triassic/Jurassic boundary. Palaeogeogr. Palaeoclimatol. Palaeoecol. 308, 418–432.
Steinthorsdottir, M., Woodward, F.I., Surlyk, F., McElwain, J.C., 2012. Deep-time evidence of a link between elevated CO_2 concentrations and perturbations in the hydrological cycle via drop in plant transpiration. Geology 40 (9), 815–818.
Steinthorsdottir, M., Elliott-Kingston, C., Bacon, K.L., 2017. Cuticle surfaces of fossil plants as a potential proxy for volcanic SO_2-emissions: observations from the Triassic–Jurassic transition of East Greenland. Palaeobiodiv. Palaeoenviron. https://doi.org/10.1007/s12549-017-0297-9.
Streel, M., Bless, M.J.M., 1980. Occurrence and significance of reworked palynomorphs. Med. Rijks Geol. Dienst. 32, 69–80.
Them, T.R., Gill, B.C., Selby, D., Grocke, D.R., Friedman, R.M., Owens, J.D., 2017. Evidence for rapid weathering response to climatic warming during the Toarcian Oceanic Anoxic Event. Sci. Rep. 7 (1), 5003.
Thiry, M., 2000. Palaeoclimatic interpretation of clay minerals in marine deposits: an outlook from the continental origin. Earth Sci. Rev. 49, 201–221.
Truswell, E.M., Drewry, D.J., 1984. Distribution and provenance of recycled palynomorphs in surficial sediments of the Ross Sea, Antarctica. Mar. Geol. 59, 187–214.
Twiddle, C.L., Bunting, M.J., 2010. Experimental investigations into the preservation of pollen grains: a pilot study of four pollen types. Rev. Palaebot. Palynol. 162, 621–630.
Uhl, D., Montenari, M., 2011. Charcoal as evidence of palaeo-wildfires in the late Triassic of SW Germany. Geol. J. 46 (1), 34–41.
van de Schootbrugge, B., 2010. A fiery start to the Jurassic. Nat. Geosci. 3 (6), 381–382.
van de Schootbrugge, B., Wignall, P.B., 2016. A tale of two extinctions: converging end-Permian and end-Triassic scenarios. Geol. Mag. 153 (02), 332–354.
van de Schootbrugge, B., Tremolada, F., Bailey, T.R., Rosenthal, Y., Feist-Burkhardt, S., Brinkhuis, H., Pross, J., Kent, D.V., Falkowski, P.G., 2007. End-Triassic calcification crisis and blooms of organic-walled disaster species. Palaeogeogr. Palaeoclimatol. Palaeoecol. 244, 126–141.
van de Schootbrugge, B., Quan, T., Lindström, S., Püttmann, W., Heunisch, C., Pross, J., Fiebig, J., Petschick, R., Röhling, H.-G., Richoz, S., Rosenthal, Y., Falkowski, P.G., 2009. Floral changes across the Triassic-Jurassic boundary linked to flood basalt volcanism. Nat. Geosci. 2, 489–594.
van de Schootbrugge, B., Richoz, S., Pross, J., Luppold, F.W., Hunze, S., Wonik, T., Blau, T., Meister, C., van der Weijst, C.M.H., Suan, G., Fraguas, A., Fiebig, J., Herrle, J.O., Guex, J., Little, C.T.S., Wignall, P.B., Püttmann, W., Oschmann, W., 2019. The Schandelah Scientific Drilling Project: a 25-million year record of early Jurassic palaeo- environmental change from northern Germany. Newsl. Stratigr. 52, 249–296.
van Eldijk, T.J.B., Wappler, T., Strother, P.K., van der Weijst, C.M.H., Rajaei, H., Visscher, H., van de Schootbrugge, B., 2018. A Triassic-Jurassic window into the evolution of Lepidoptera. Sci. Adv. 4, e1701568.
Van Nuland, M.E., Wooliver, R.C., Pfennigwerth, A.A., Read, Q.D., Ware, I.M., Mueller, L., Fordyce, J.A., Schweitzer, J.A., Bailey, J.K., Fox, C., 2016. Plant-soil feedbacks: connecting ecosystem ecology and evolution. Funct. Ecol. 30 (7), 1032–1042.
Vavrdová, M., 2008. Proterozoic acritarchs from the Precambrian-Cambrian transition in southern Moravia. Bull. Geosci. 83, 85–92.
Visscher, H., Brinkhuis, H., Dilcher, D.L., Elsik, W.C., Eshet, Y., Looy, C.V., Rampino, M.R., Traverse, A., 1996. The terminal Paleozoic fungal event: evidence of terrestrial ecosystem destabilisation. Proc. Natl. Acad. Sci. 93, 2155–2158.
von Hildebrandt, L., Schweizer, V., 1992. Zur biostratigraphischen Gliederung des Unteren Jura in der Langenbrückener Senke (Baden-Württemberg, Südwestdeutschland). In: Jahresbericht und Mitteilungen der oberrheinischen geologischen Verein, NF. 74. pp. 215–236.
Vorob'eva, N.G., Sergeev, V.N., Knoll, A.H., 2009. Neoproterozoic microfossils from the Northeastern margin of the east European Platform. J. Paleontol. 83, 161–196.
Wang, C., Visscher, H., 2007. Abundance anomalies of aromatic biomarkers in the Permian–Triassic boundary section at Meishan, China — evidence of end-Permian terrestrial ecosystem collapse. Palaeogeogr. Palaeoclimatol. Palaeoecol. 252 (1–2), 291–303.
Wignall, P.B., Bond, D.P.G., Kuwahara, K., Kakuwa, Y., Newton, R.J., Poulton, S.W., 2010. An 80 million year oceanic redox history from Permian to Jurassic pelagic sediments of the Mino-Tamba terrane, SW Japan, and the origin of four mass extinctions. Glob. Planet. Chang. 71 (1–2), 109–123.
Wilmshurst, J.M., McGlone, M.S., 2005. Corroded Pollen and Spores as Indicators of changing Lake Sediment sources and Catchment Disturbance. J. Palaeolimnol. 34 (4), 503–517.
Wilson, L.R., 1964. Recycling, stratigraphic leakage, and faulty techniques in palynology. Grana 5, 425–436.
Windle, T.M.F., 1979. Reworked carboniferous spores: An example from the lower Jurassic of Northeast Scotland. Rev. Palaebot. Palynol. 27, 173–184.
Zajzon, N., Kristaly, F., Palfy, J., Nemeth, T., 2012. Detailed clay mineralogy of the Triassic-Jurassic boundary section at Kendlbachgraben (Northern Calcareous Alps, Austria). Clay Miner. 47, 177–189.
Zhu, Z., Liu, Y., Kuang, H., Benton, M.J., Newell, A.J., Xu, H., An, W., Ji, S., Xu, S., Peng, N., Zhai, Q., 2019. Altered fluvial patterns in North China indicate rapid climate change linked to the Permian-Triassic mass extinction. Sci. Rep. 9 (1), 16818.
Ziegler, P.A., 1990. Geological atlas of western and central Europe. In: Shell International Petroleum Maatschappij, pp. 239.